Rocks & Stars II Conference, Max-Planck-Institut für Sonnensystemforschung

Göttingen, Sept. 13 – 16, 2017

Why numerical simulations?

Oskar Steiner

Kiepenheuer-Institut für Sonnenphysik, Freiburg i.Br., Germany

Istituto Ricerche Solari Locarno (IRSOL), Locarno Monti, Switzerland

Table of content

Part I: Aspects of computational astrophysics

§ 1. The role of computer simulations in astrophysics

References

Part II: MHD simulations: Case studies

§ 2. Observations vs. simulations of the solar atmosphere

§ 3. *Case study I:* Interpretation of polarimetric signals

§ 4. *Case study II:* The discovery of non-magnetic bright points

§ 5. *Case study III:* Virtual experiments with numerical simulations

§ 5.1. Magnetic halos and shadows

§ 5.2. Gravity waves

§ 6. Small-scale magnetism of main sequence stellar atmospheres

References

Part I: Aspects of computational astrophysics

§ 1 The role of computer simulations in astrophysics

Historical Perspective:

- 1950's and 1960's: Stellar evolution calculations (Martin Schwarzshild in the U.S. and Rudolph Kippenhahn in Göttingen, Germany). At that time *computers were viewed as tools for the numerical integration* rather than as a tool for experimentation.

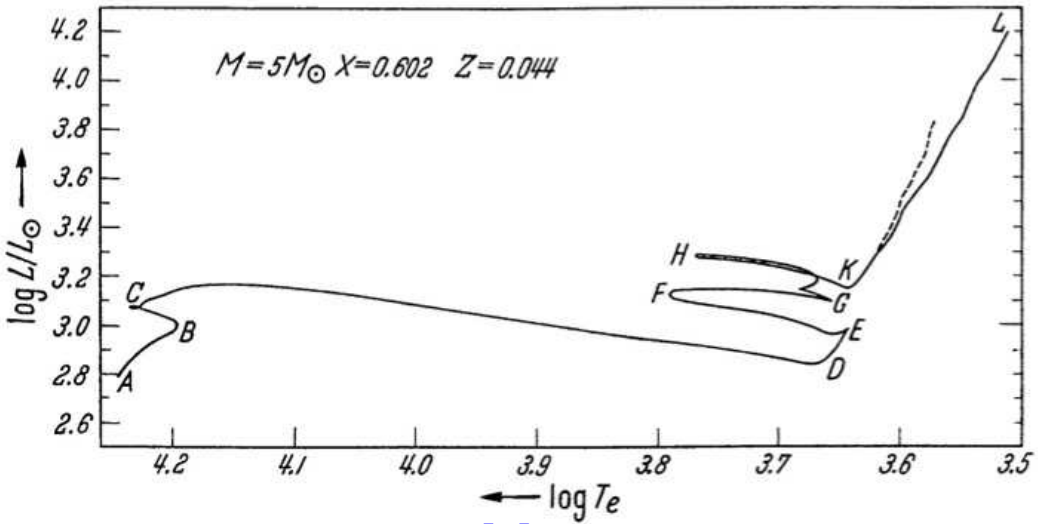

Evolution of a 5 $M_\odot$ star in the HRD

Kippenhahn et al. (1965, Zeitschrift für Astrophysik)

Rudolph Kippenhahn

1. The role of computer simulations in astrophysics (cont.)

- 1960's: N-body stellar dynamics simulations (e.g. tidal interaction of galaxies) and hydrodynamical systems (e.g. core collapse supernovae). Notion of *computational astrophysics as experimental astronomy*.

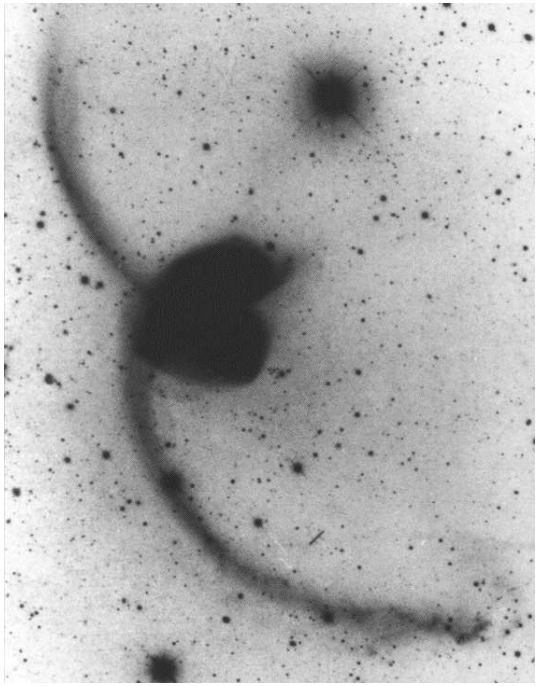

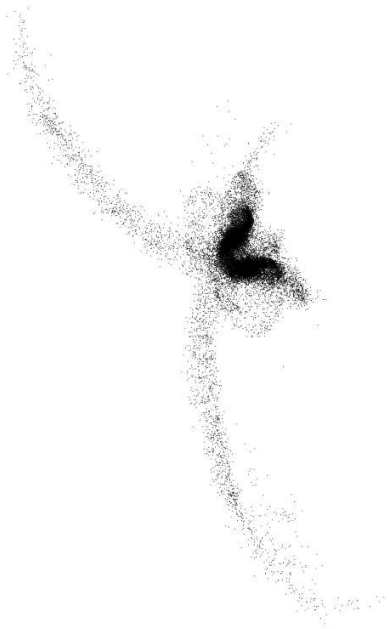

The antenna nebula NGC 4038/4039 evolved from a collision of two similarly sized spiral galaxies. *Left:* Observed present state. *Right:* Present state from a computer simulation of the complete collision (www.ifa.hawaii.edu/~barnes).

These simulations are generally *motivated by the question "What happens if?"* more so than "What is the solution to these equations?".

Computational astrophysics is the experimentation with astrophysical objects in a virtual (numerical) laboratory, comparable to the manipulation with real probes in classical physics experiments.

Role of Computational astrophysics:

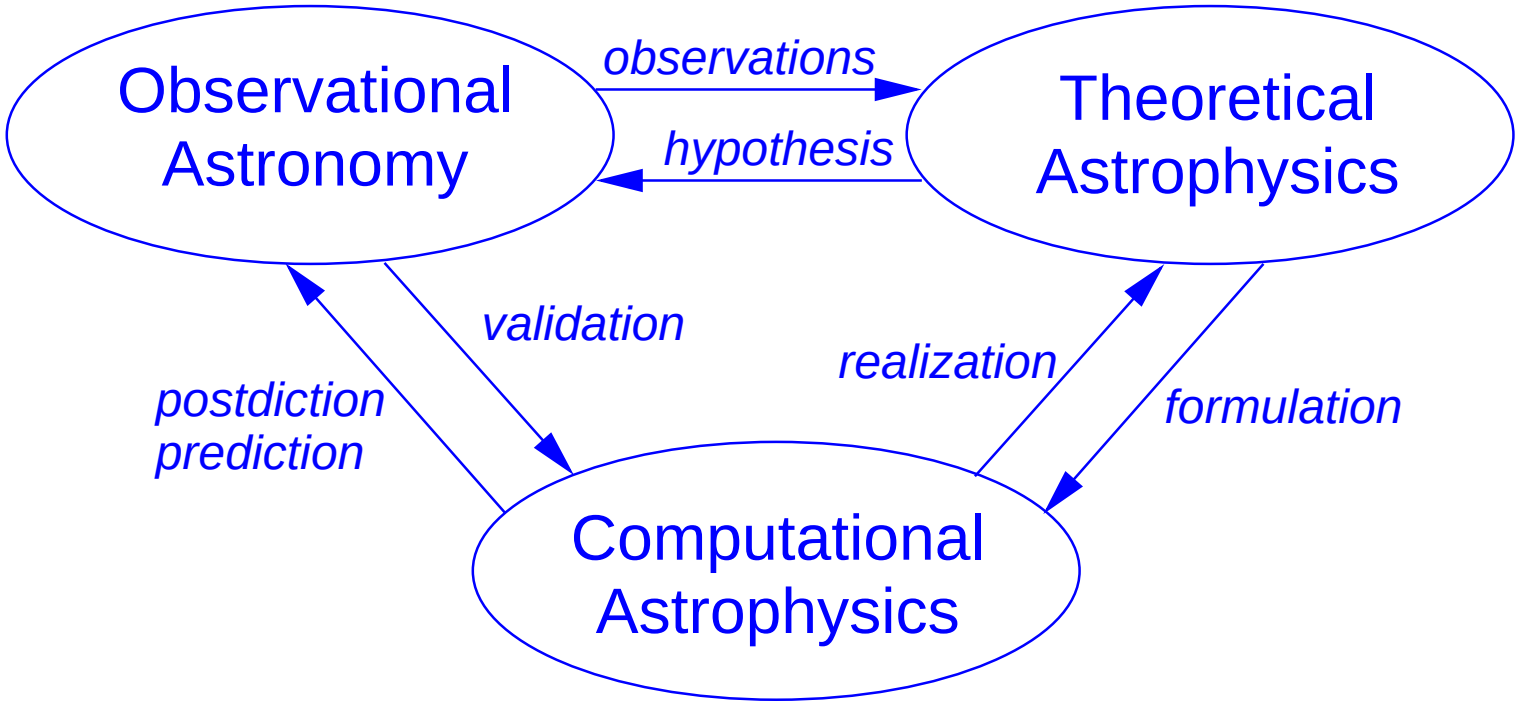

Adapted from *M. Norman (1997)*

1. The role of computer simulations in astrophysics (cont.)

Simulations tend to model a *time dependent* physical system with some degree of *realism*. Usually, simulated systems have no simple closed form analytic solutions. Otherwise, one rather talks of *modeling*.

Realistic simulations produce observable quantities like intensity maps or polarimetric maps that look like corresponding actual observations, so called *virtual or synthetic observations*. Typically, a realistic solar simulation uses a *realistic equation of state* that takes ionization and the composition of the solar plasma into account and it carries out *radiation transfer with actual opacities* as occurring in the solar plasma.

References

Kippenhahn, R., Thomas, H.-C., and Weigert, A.: 1965, Sternetnwicklung IV. Zentrales Wasserstoff- und Heliumbrennen bei einem Stern von 5 Sonnenmassen, Zeitschrift für Astrophysik 61, 241-267

Kippenhahn, R.: 2008, Als die Computer die Astronomie eroberten, Reviews in Modern Astronomy 20, 1-14

Norman, M.: 1997, Computational Astrophysics: The “New Astronomy” for the 21st Century, in ASP Conf. Series Vol. 123, D.A. Clarke & M.J. West (eds.), p. 3-14

Ostriker, J.P.: 2000, Historical Reflection on the Role of Numerical Modeling in Astrophysics, Reviews in Modern Astronomy 13, 1-11

Part II: MHD simulations: Case studies

§ 2 Observations vs. simulations of the solar atmosphere

The solar atmosphere is in continuous turbulent motion. Light that reaches us from the Sun bears information on this dynamics and it's magnetic field. But this information is not easy to decipher. *Numerical simulations* help us to do this.

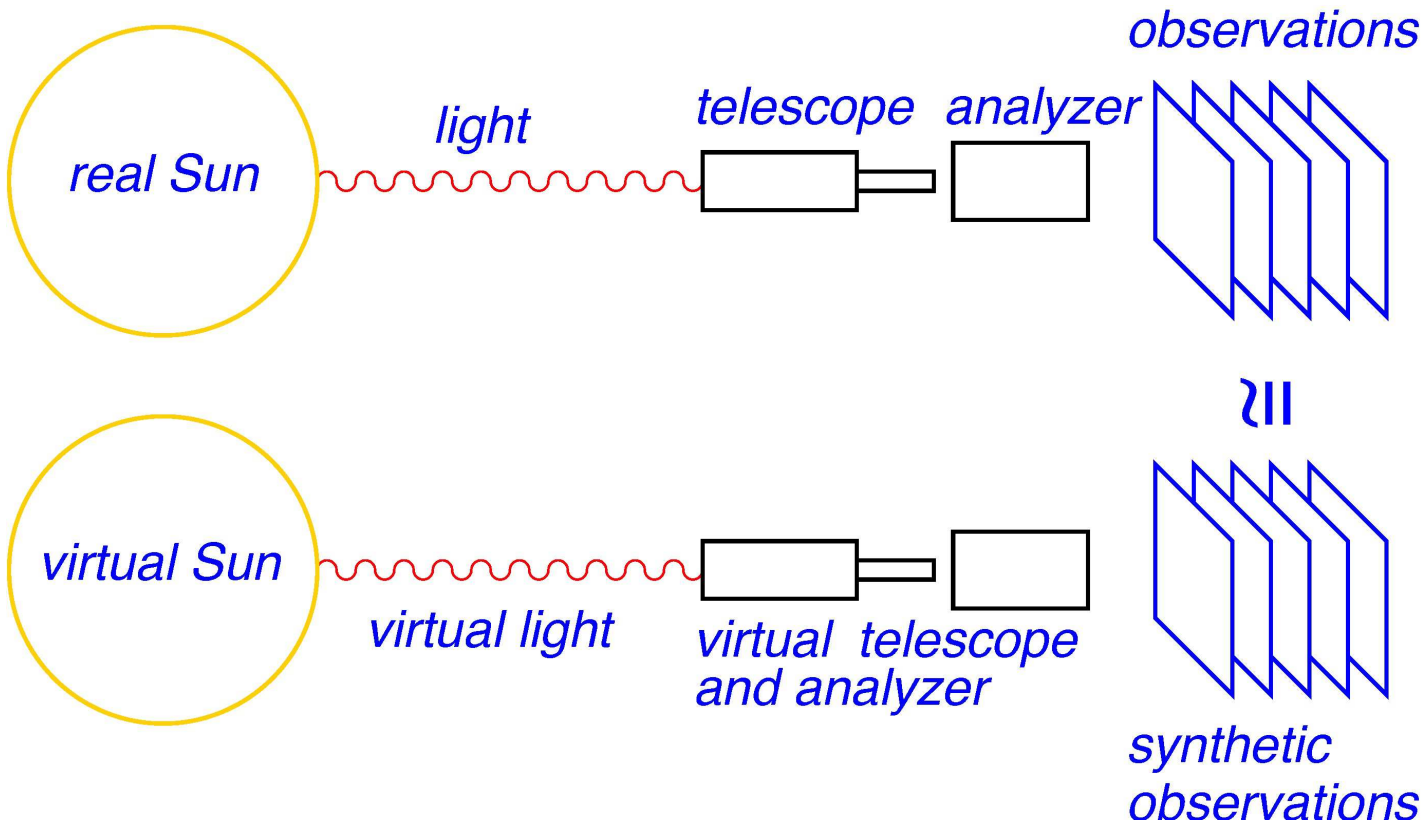

2. Observations vs. simulations of the solar atmosphere (cont.): nMBPs

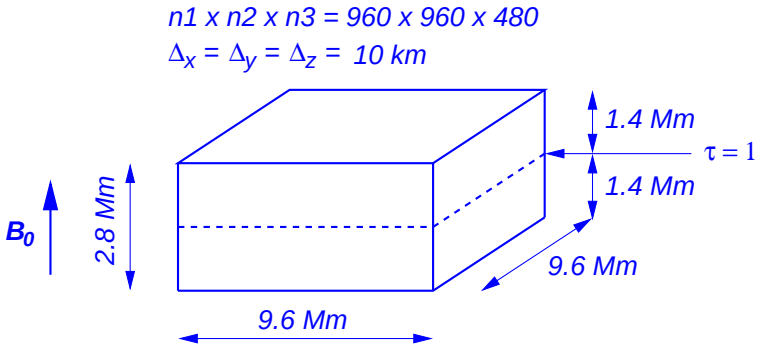

convection zone

convection zone base

Size of a typical three-dimensional computational domain in comparison with the size of the Sun.

2. Observations vs. simulations of the solar atmosphere (cont.)

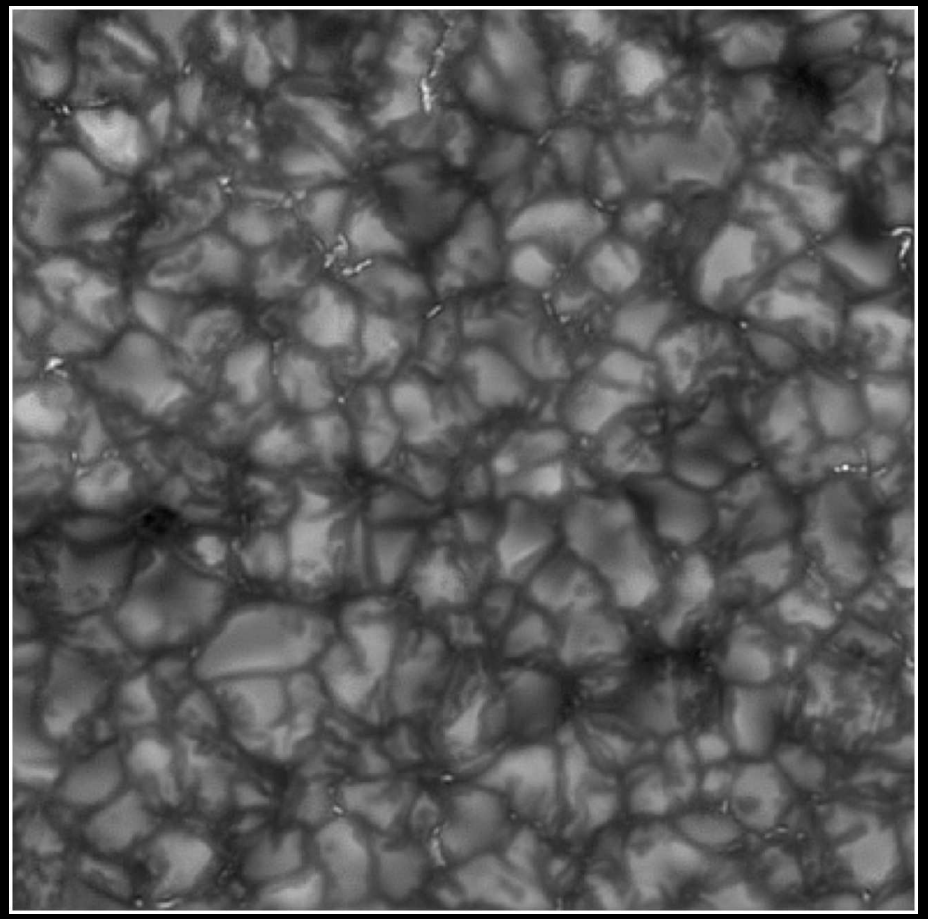

Observation of the solar surface

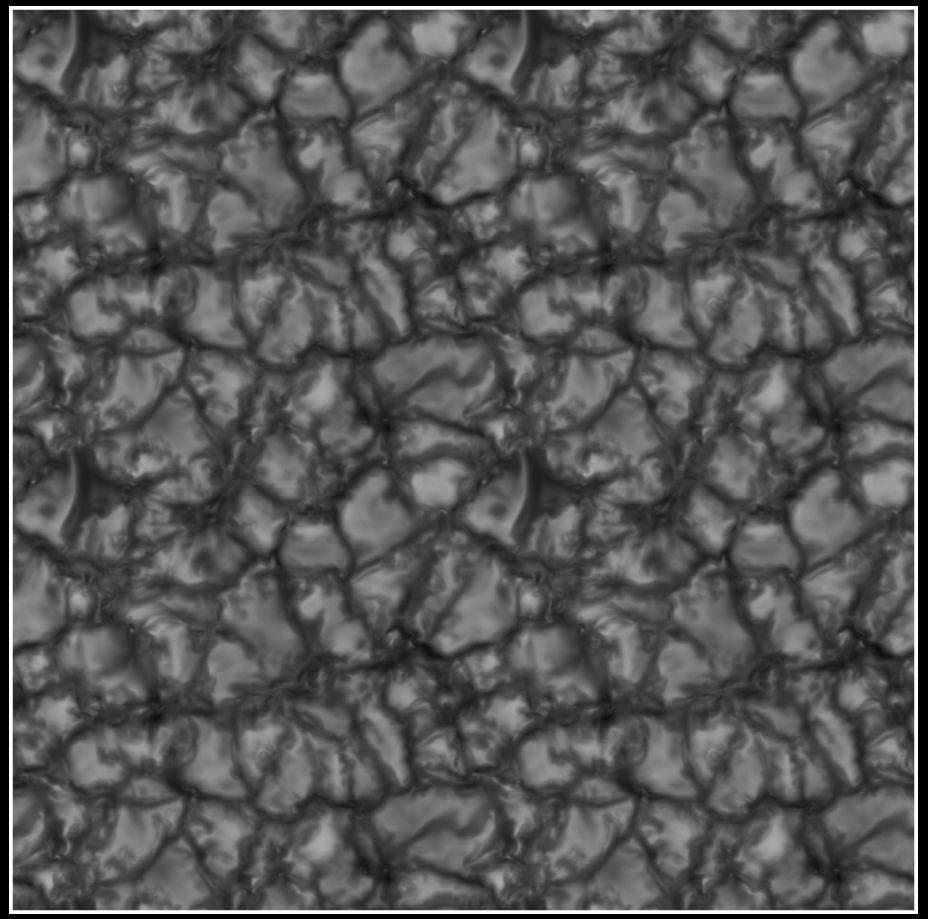

Numerical simulation

§ 3 *Case study I:* Interpretation of polarimetric signals

Case study I is a typical example of *post diction*: Something that was observed is *reproduced with simulations*, which helps us to better understand and interpret the observation.

3. *Case study I:* Interpretation of polarimetric signals (cont.)

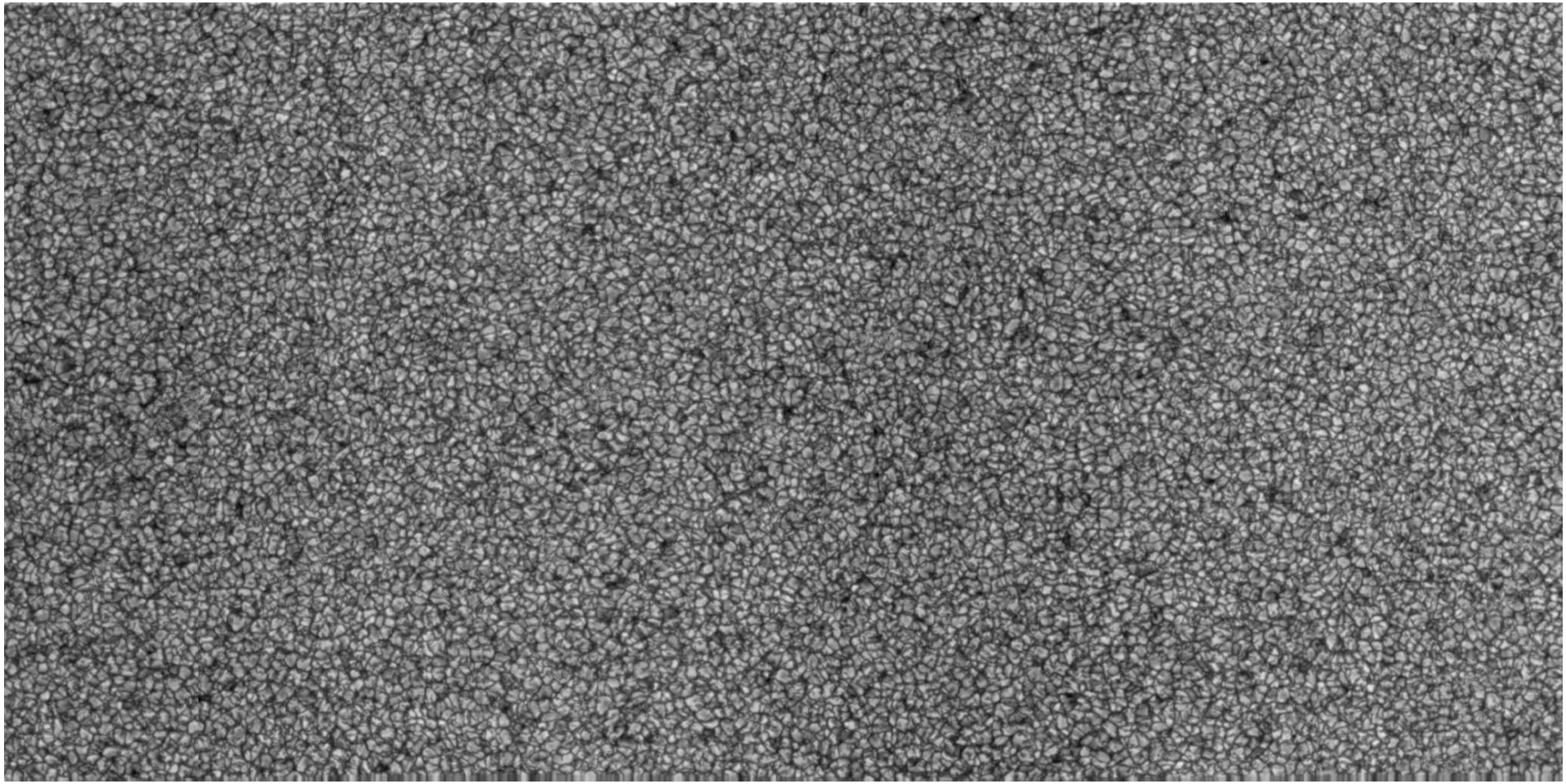

Continuum intensity at 630 nm over a field of view of $302'' \times 162''$ recorded with Hinode/SOT/SP. 2048 slit positions. From *Lites et. al. 2008, ApJ 672, 1237*

3. *Case study I:* Interpretation of polarimetric signals (cont.)

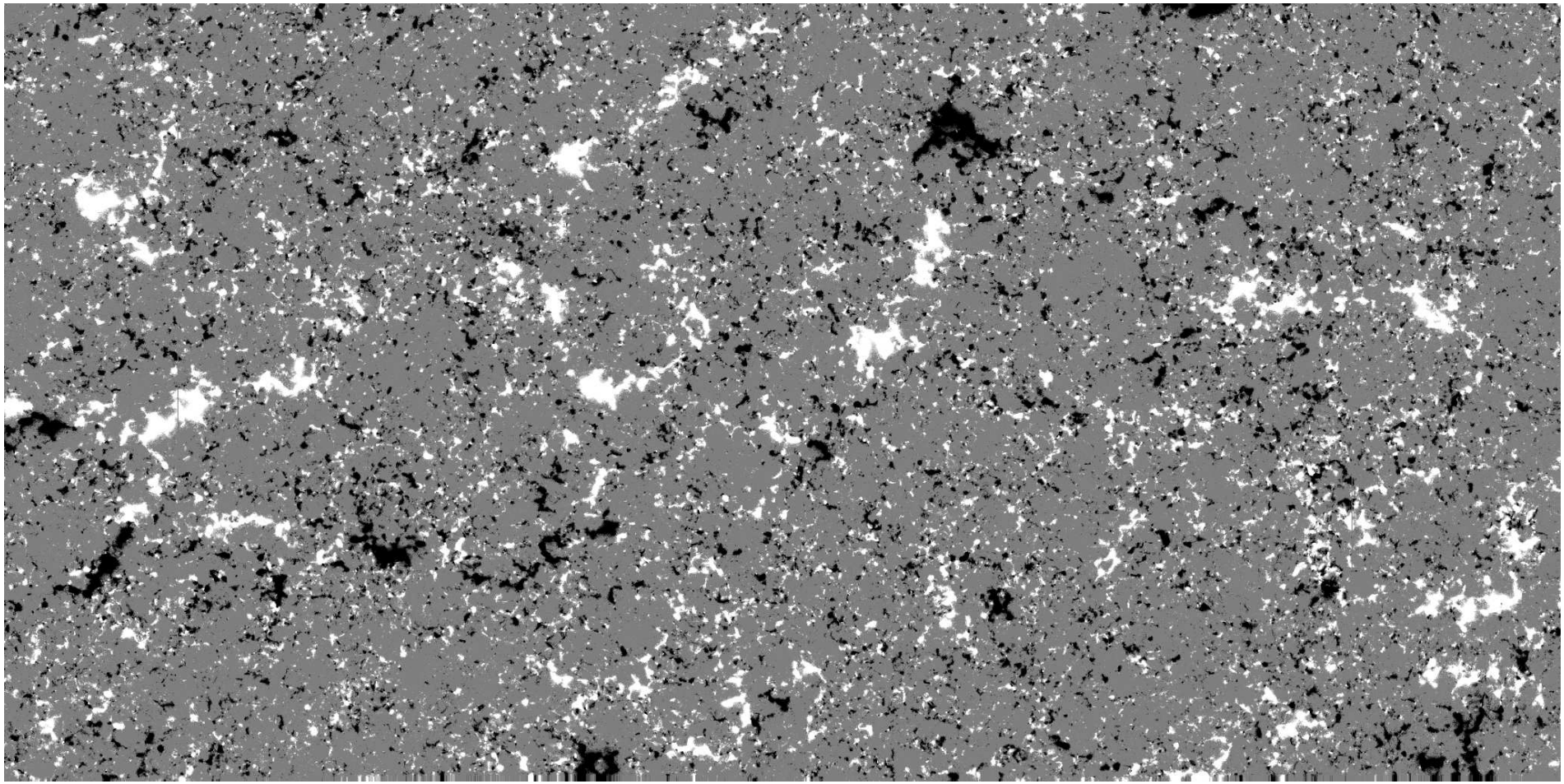

Apparent vertical magnetic flux density, $B^{\rm L}_{\rm app}$, of the quiet Sun over a field of view of $302'' \times 162''$. 2048 steps to 4.8 s. Maps of Fe I 630.15 and 630.25 nm.

From *Lites et. al. 2008, ApJ 672, 1237*

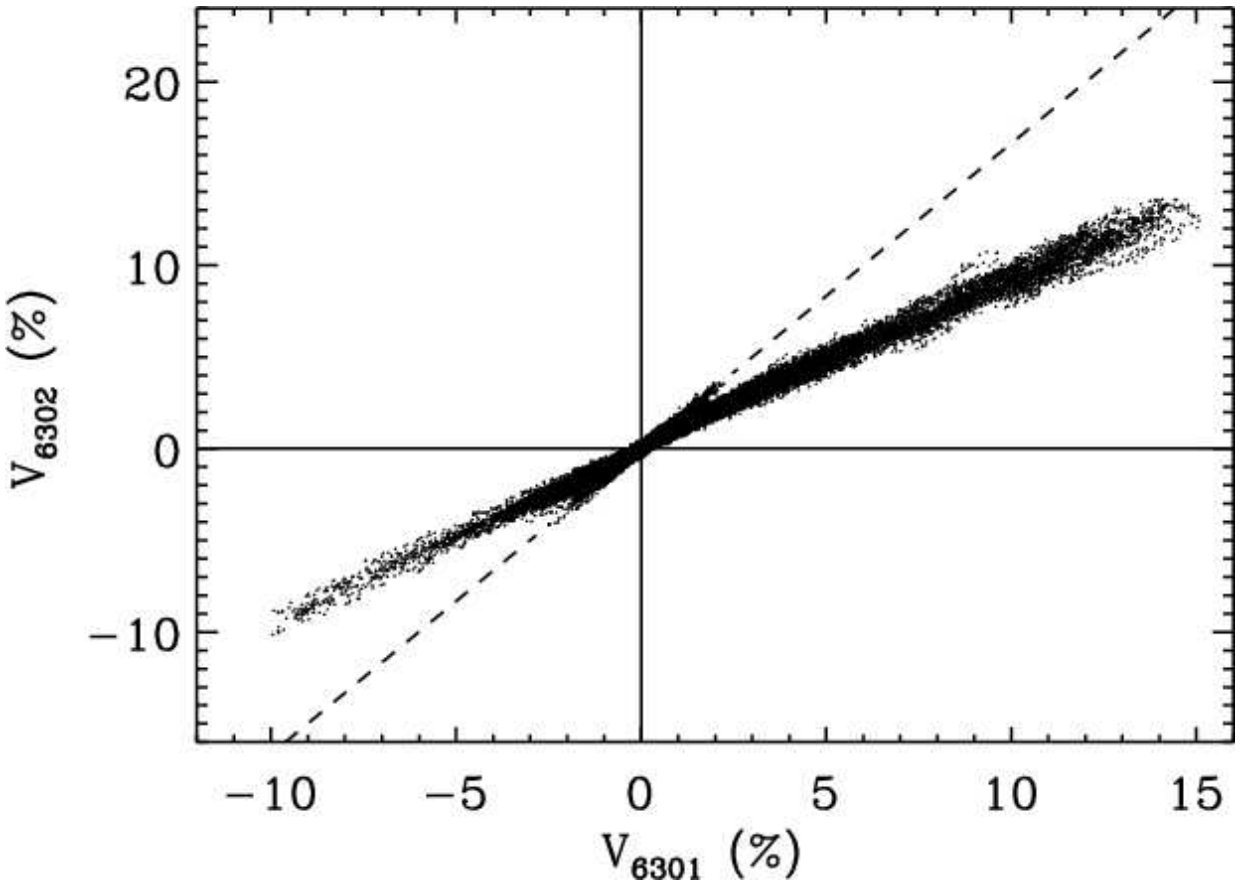

Scatter plot of the blue lobe Stokes-V amplitudes of the 6302.5 Å line vs. the 6301.5 Å line as *observed with Hinode/SOT/SP*. The dashed line is the regression relation expected for weak magnetic fields. We identify two populations of points. From *Stenflo (2011) A&A 529 A42*. ⇒ Section at 1%

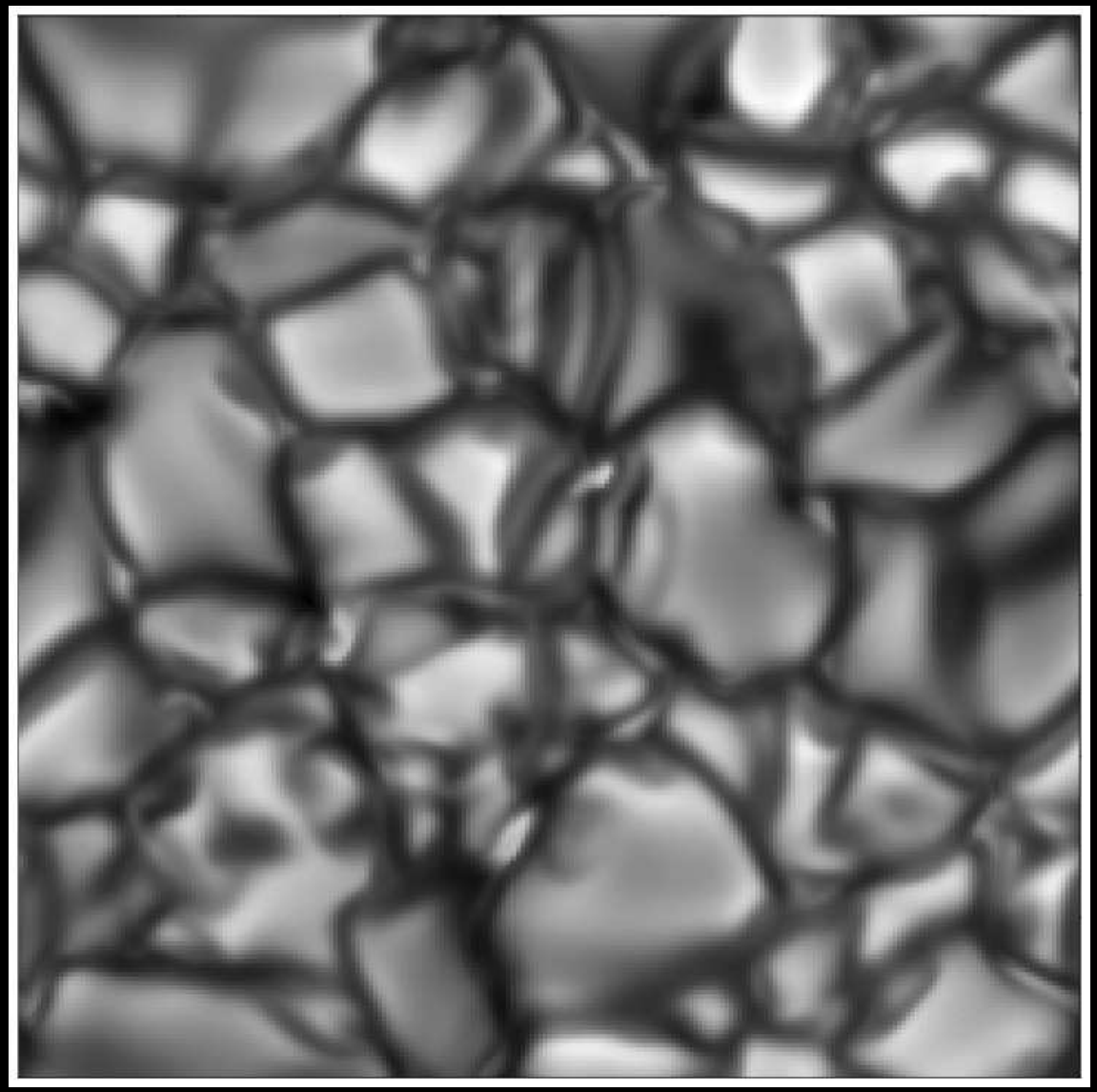

3. *Case study I:* Interpretation of polarimetric signals (cont.): simulation data

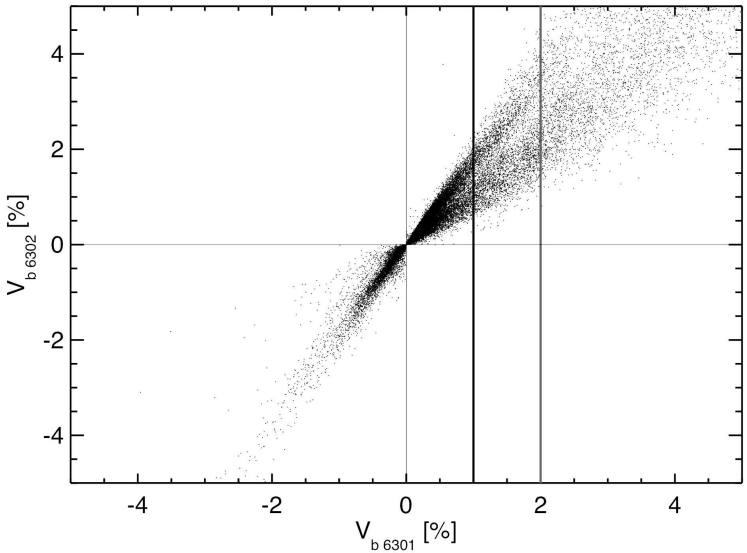

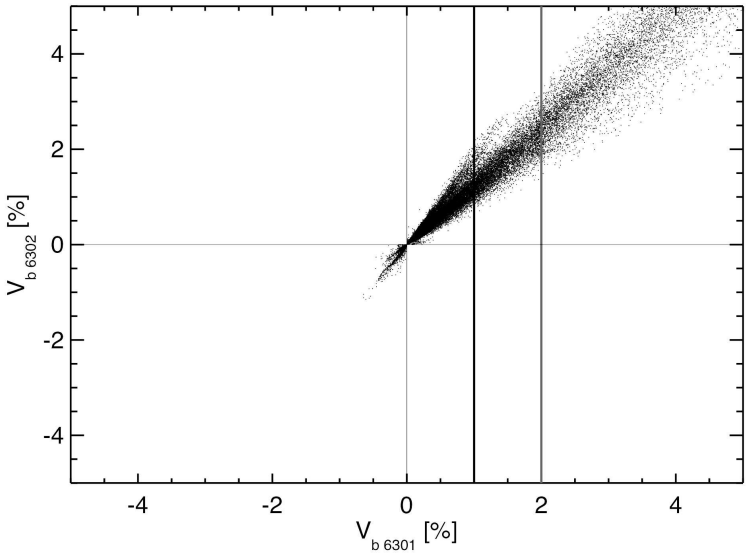

Scatter plot of the Stokes-V line ratio from the simulation. *Left:* full resolution;

Right: degraded with the SOT/SP point spread function. From *Steiner & Rezaei (2012)*.

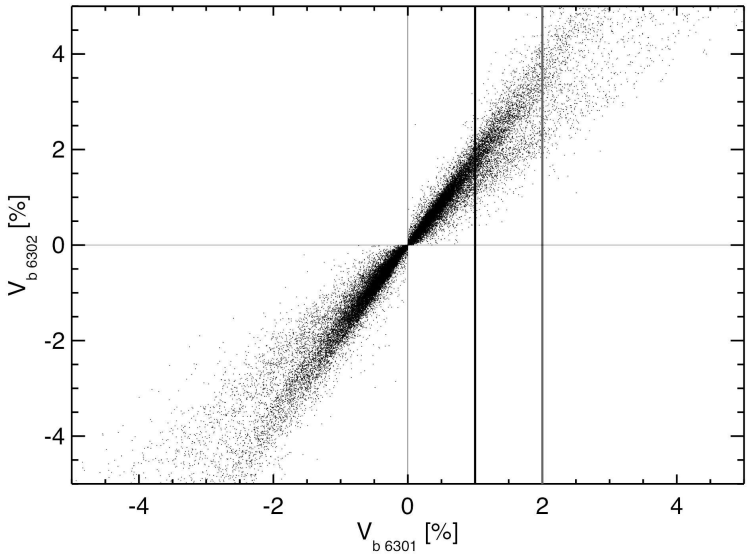

Scatter plot of the Stokes-V line ratio from a mixed polarity simulation.

“It is nice to know that the computer understands the problem, but I would like to understand it too.”

Attributed to E.P. Wigner

meaning:

“It is nice to know that our simulations reproduce the observations, but what can we learn from it?”

3. *Case study I:* Interpretation of polarimetric signals (cont.)

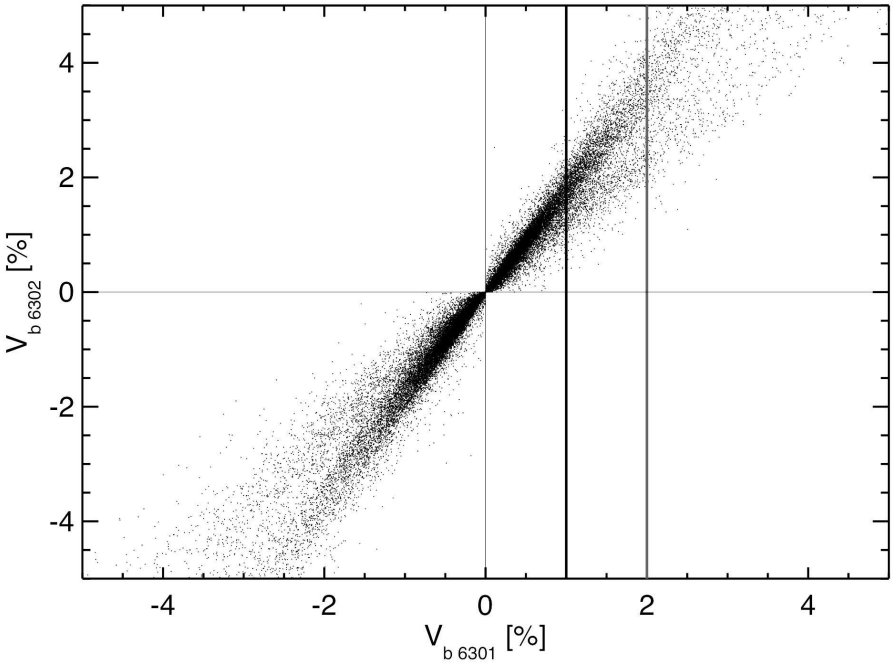

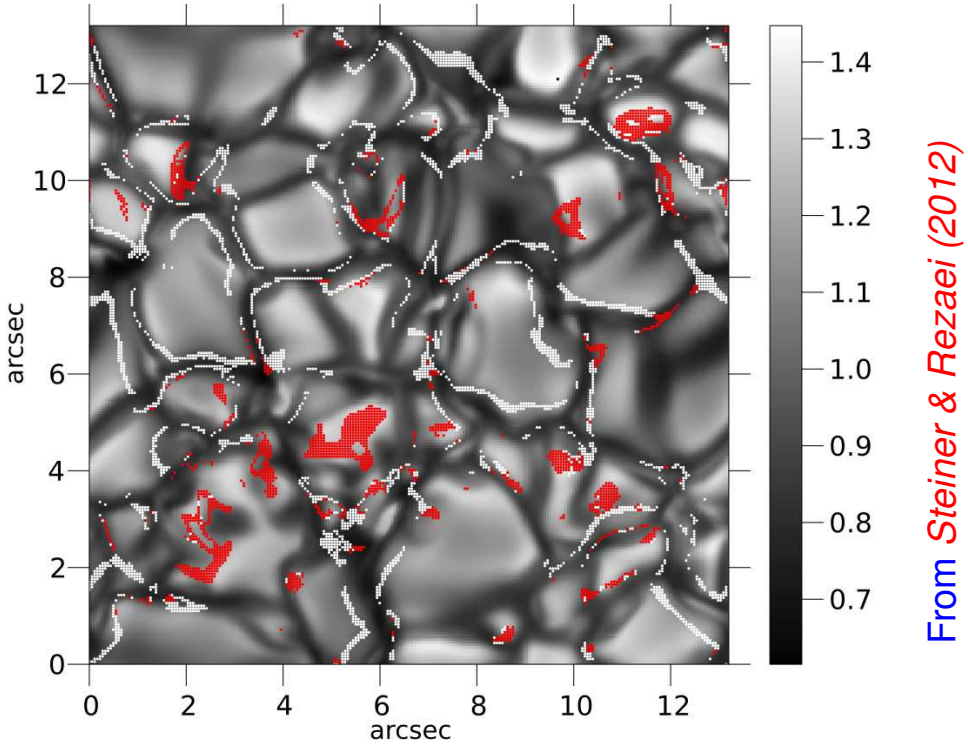

From *Steiner & Rezaei (2012)*

Conclusion: The two populations can be explained in terms of weak (hectogauss) magnetic fields. *Numerical simulations are indispensable for the correct interpretation.*

Maurizio Nannucci, Neon installation in the court of the Museo Novecento, Florence

Case study I is a typical example of *post diction*: Something that was observed got *reproduced by simulations*, which helped us to better understand and interpret the observation.

The next paragraph treats an example of *prediction*.

§ 4 *Case study II:* The discovery of non-magnetic bright points

Bolometric intensity maps

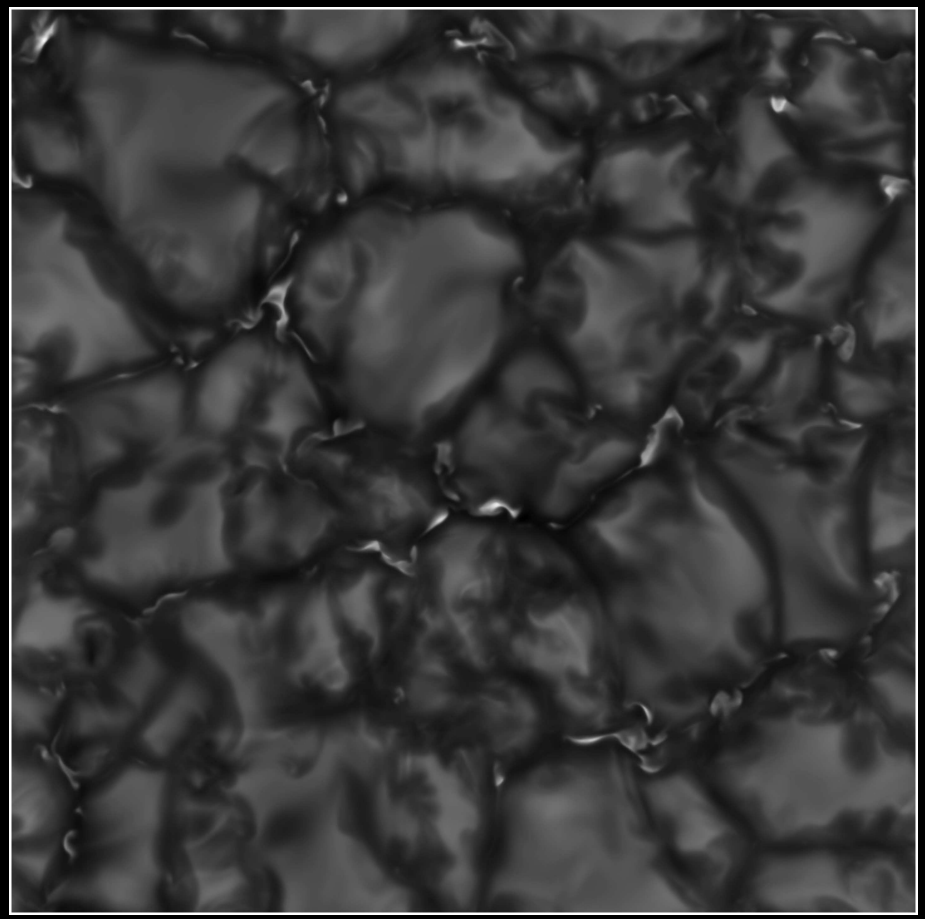

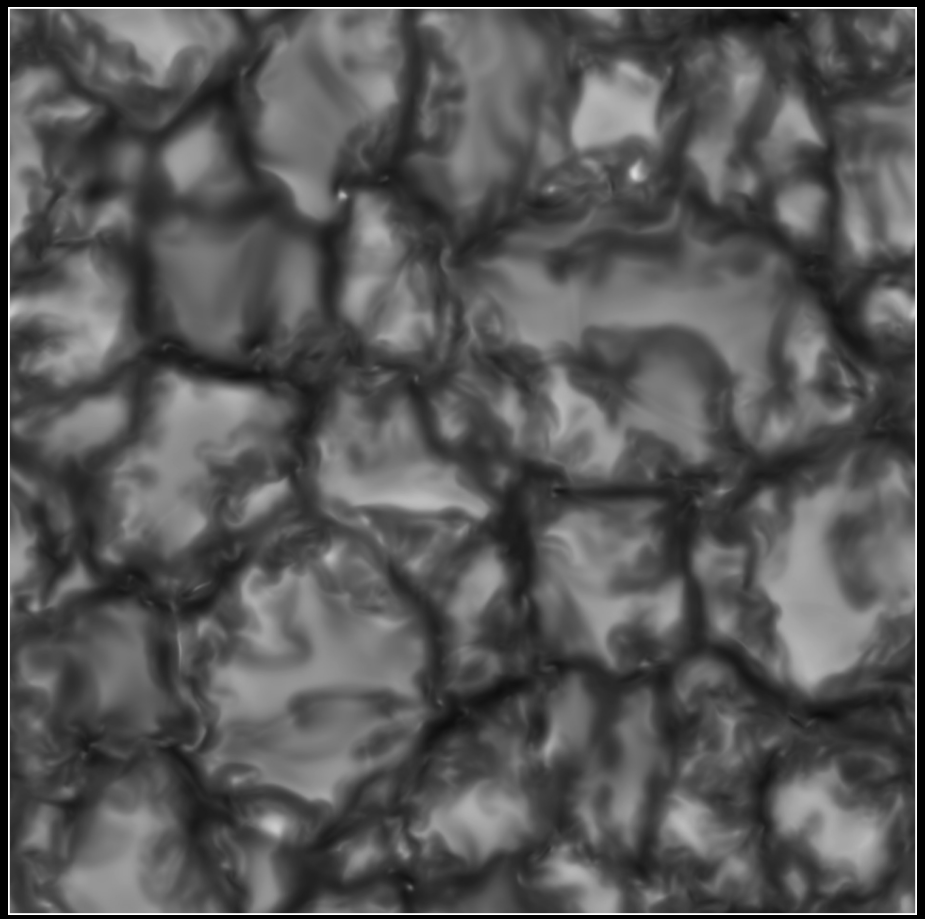

Computations: *Centro Svizzero di Calcolo Scientifico*

With magnetic fields:
Magnetohydrodynamic simulation

Without magnetic fields:
Hydrodynamic simulation

Courtesy,
F. Calvo

4. *Case study II:* The discovery of non-magnetic bright points (cont.)

Slices across a non-magnetic bright point (nMBP0868)

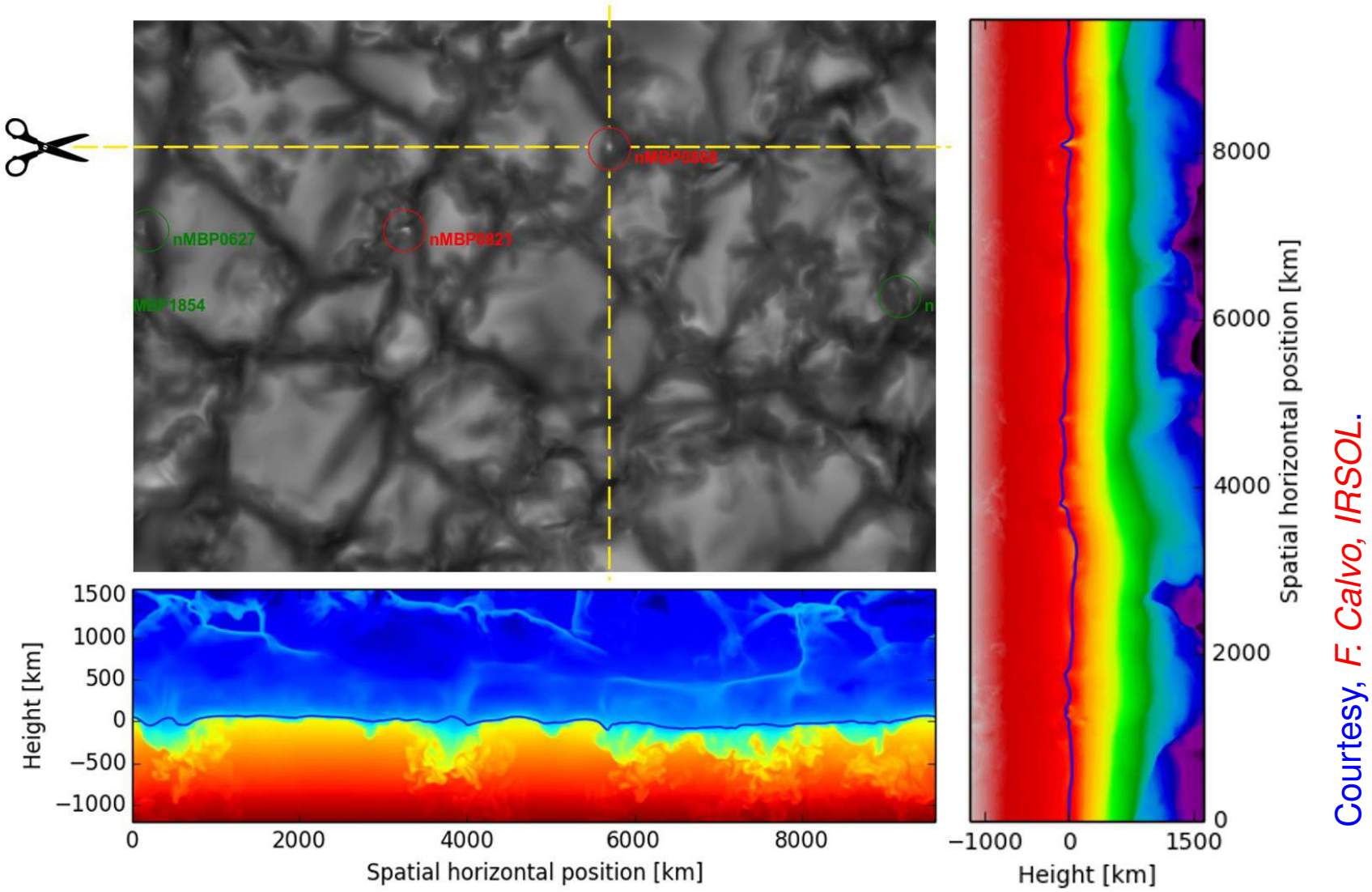

Courtesy, *F. Calvo, IRSOL.*

Emergent intensity I (*top left*), temperature T (*bottom*), density $\log(\rho)$ (*right*)

4. *Case study II:* The discovery of non-magnetic bright points (cont.)

Slices across a non-magnetic bright point (nMBP0868)

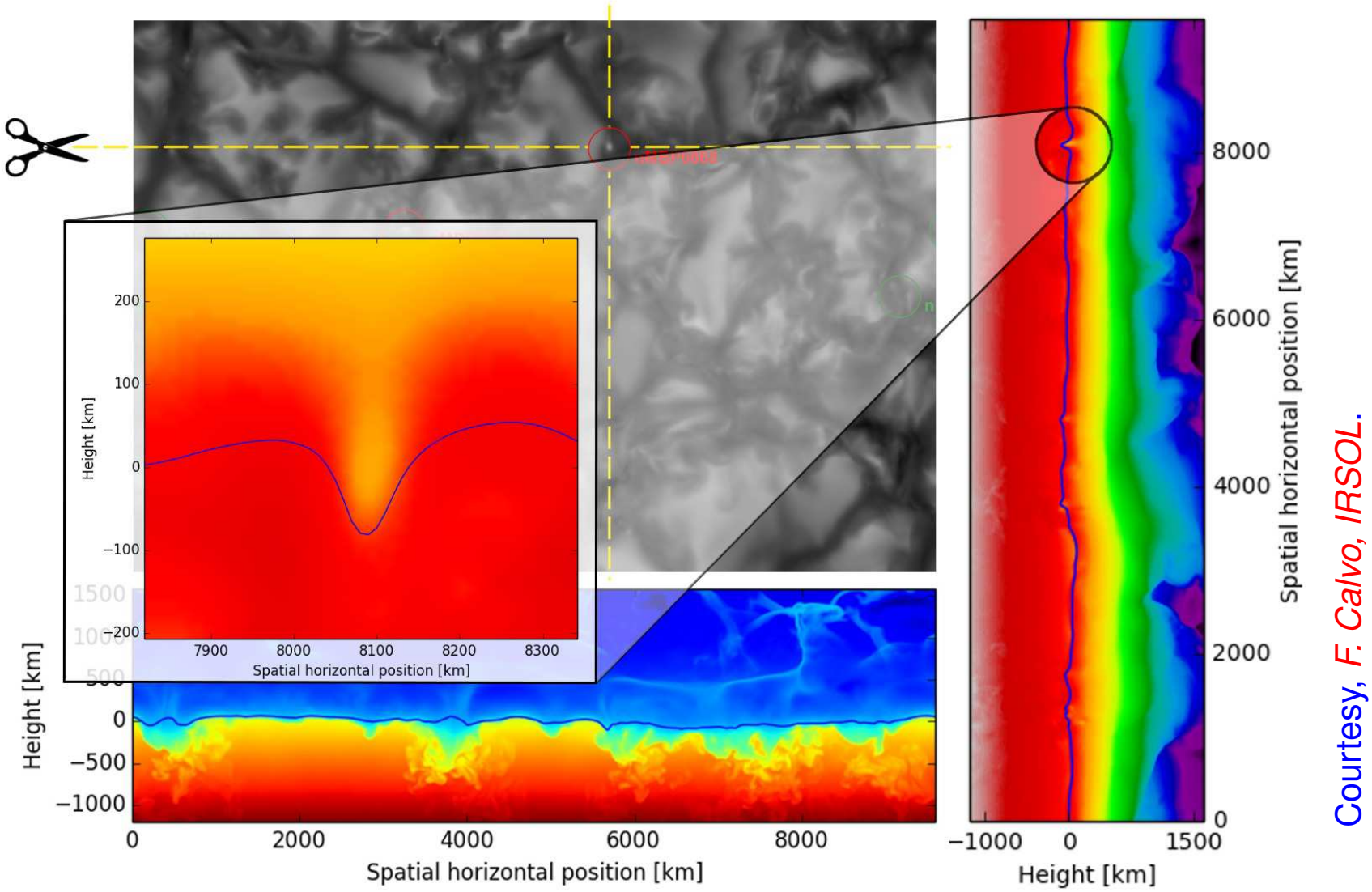

Emergent intensity I (*top left*), temperature T (*bottom*), density $\log(\rho)$ (*right*)

4. *Case study II:* The discovery of non-magnetic bright points (cont.)

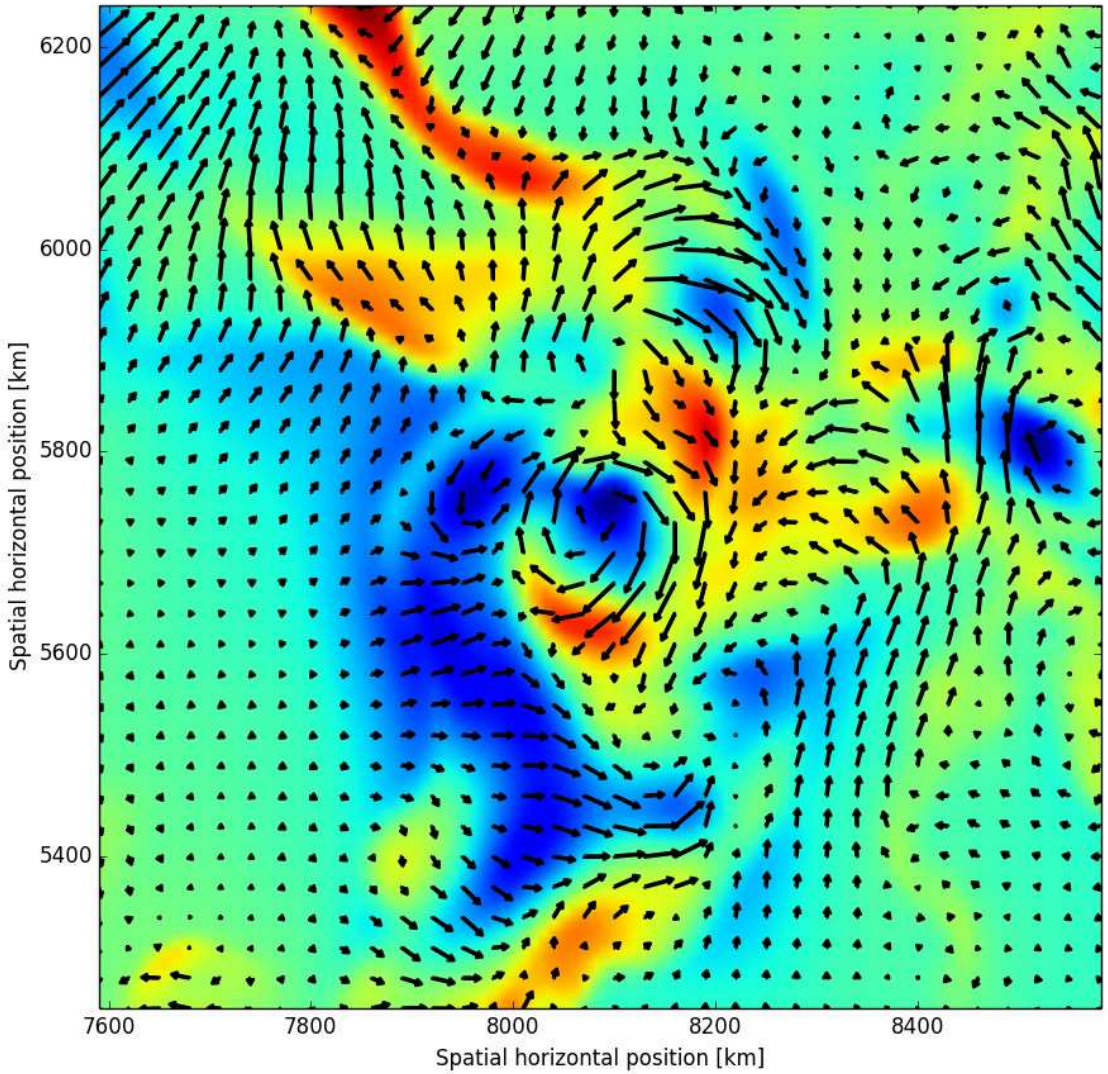

Density (blue: low, red: high) and velocity field in an horizontal plane, 150 [km] below $\langle \tau \rangle = 1$

non-magnetic bright points (nMBPs) are locations with:

- *swirling motion* (but ≈ 150 [km] below $\tau = 1$ there are often swirls that do not produce nMBPs);
- *low density* (but a density deficiency alone does not warrant nMBP's);
- *high intensity contrast* (but a local intensity peak does not need to be a nMBP).

From *F. Calvo et al. 2016*.

4. *Case study II:* The discovery of non-magnetic bright points (cont.)

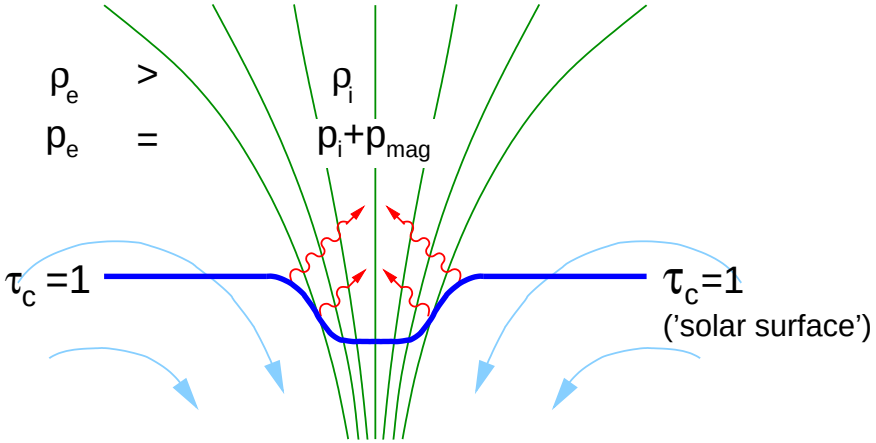

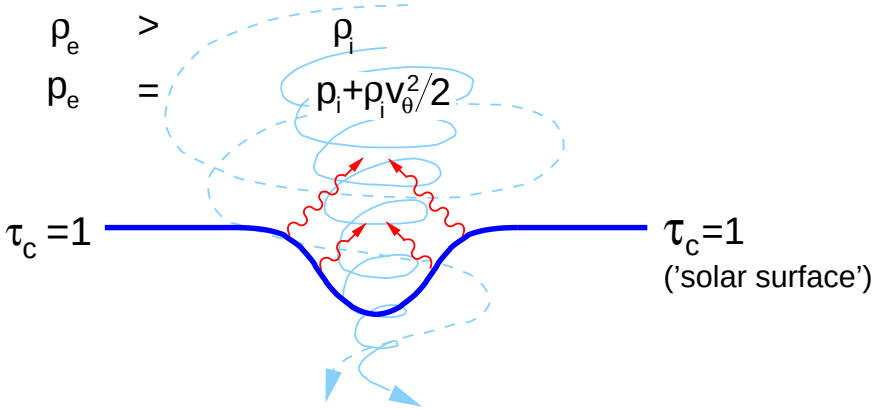

Magnetic flux sheet. Depression due to magnetic pressure.

Swirl. Depression due to centrifugal force.

In both cases is the 'hot wall effect' responsible for the enhanced radiation from the depression.

4. *Case study II:* The discovery of non-magnetic bright points (cont.)

Reduction to an analytical toy model

Starting from the momentum equation

$$\frac{\partial \boldsymbol{v}}{\partial t} + (\boldsymbol{v} \cdot \boldsymbol{\nabla})\, \boldsymbol{v} + \frac{1}{\rho} \boldsymbol{\nabla} P + \boldsymbol{g} = 0\,,$$

we assume

1. nMBPs are long-lived and stable so that the velocity field can be considered stationary;
2. They have cylindrical symmetry;
3. Their velocity field has a non-vanishing azimuthal component;
4. They extend in the vertical direction and their shape does not depend on depth.

Because of 2., the Euler momentum equation can be written in cylindrical coordinates.

Reduction to an analytical toy model

The advection term is then given by

$$(\boldsymbol{v}\cdot\boldsymbol{\nabla})\boldsymbol{v} = \left[(\boldsymbol{v}\cdot\boldsymbol{\nabla})v_r - \frac{v_\theta^2}{r}\right]\hat{\boldsymbol{r}} + \left[(\boldsymbol{v}\cdot\boldsymbol{\nabla})v_\theta + \frac{v_\theta v_r}{r}\right]\hat{\boldsymbol{\theta}} + (\boldsymbol{v}\cdot\boldsymbol{\nabla})v_z\hat{\boldsymbol{z}}\,,$$

where the directional derivative is

$$\boldsymbol{v}\cdot\boldsymbol{\nabla} = v_r\partial_r + \frac{v_\theta}{r}\partial_\theta + v_z\partial_z\,.$$

The simplest field satisfying the conditions 1–4 is $\boldsymbol{v} = v_\theta\,(r)\,\hat{\boldsymbol{\theta}}$. Inserting it into the Euler momentum equation and projecting it into the horizontal plane yields

$$\frac{\partial P}{\partial r} - \rho\frac{v_\theta^2}{r} = 0\,.$$

The pressure gradient is provided by the centripetal force.

Reduction to an analytical toy model

One can then estimate the magnitude of v_θ. With

$$\frac{P_{\rm ext} - P_{\rm int}}{\rho_{\rm ext}} \approx v_\theta^2 \,, \qquad \frac{\rho_{\rm int} - \rho_{\rm ext}}{\rho_{\rm ext}} \equiv C_\rho \,, \quad \frac{T_{\rm int} - T_{\rm ext}}{T_{\rm ext}} \equiv C_T \,,$$

$$\frac{P_{\rm ext}}{\rho_{\rm ext}} \approx R_{\rm s}\, T_{\rm ext} \,, \qquad T_{\rm ext} \approx T_{\rm eff} \,,$$

one obtains with $C_\rho \approx -0.5$ and $C_T \approx 0$

$$v_\theta = \sqrt{R_{\rm s}\, T_{\rm eff}\, [1 - (1 + C_\rho)(1 + C_T)]} \approx \sqrt{\frac{R_{\rm s}\, T_{\rm eff}}{2}} = 4.4\,{\rm km\,s^{-1}} \,,$$

while the maximum azimuthal velocities in the simulation are $v_\theta^{\rm max} \approx 6\,{\rm kms}^{-1}$.

4. *Case study II:* The discovery of non-magnetic bright points (cont.)

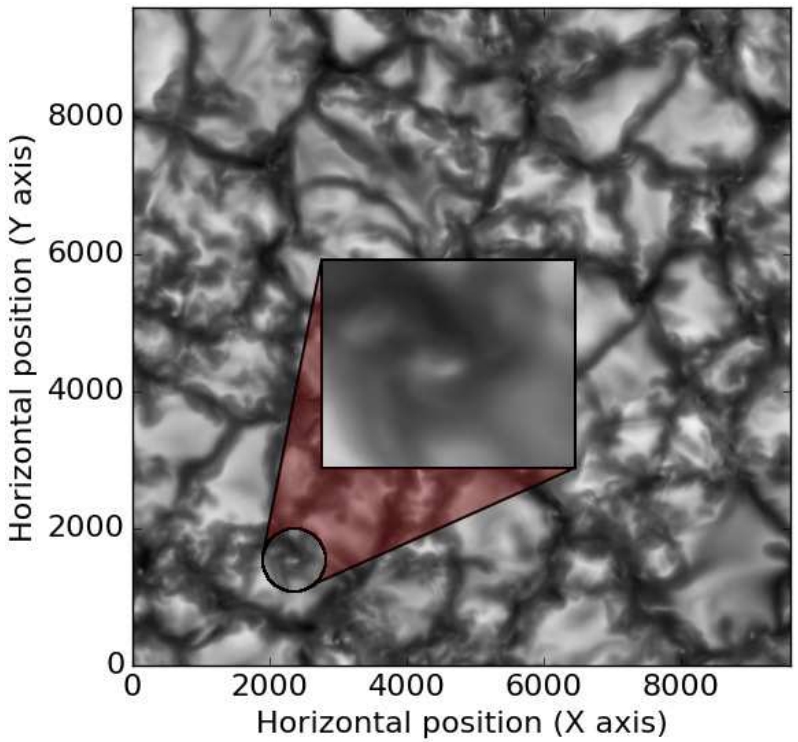

full resolution

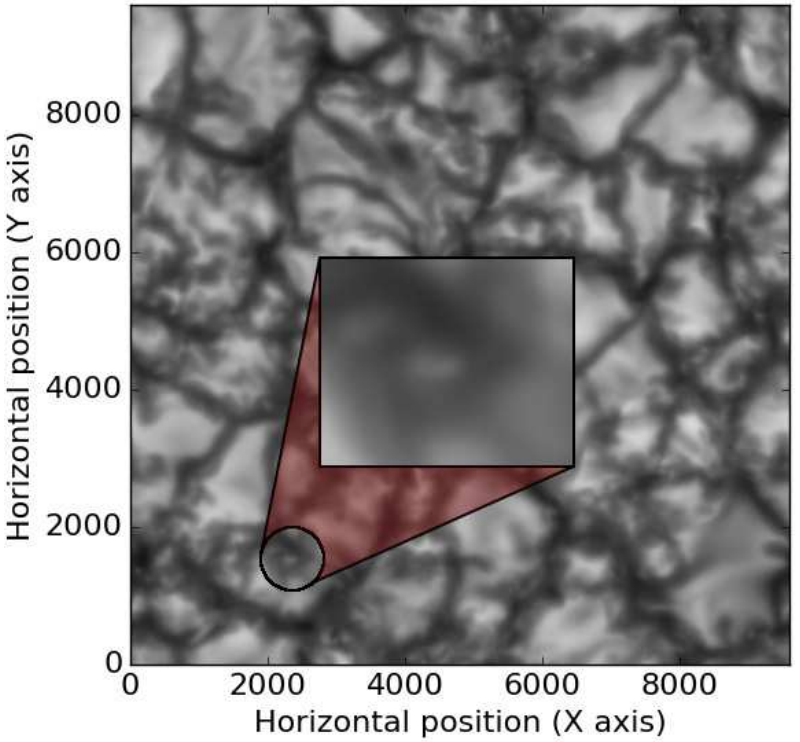

Gregor resolution

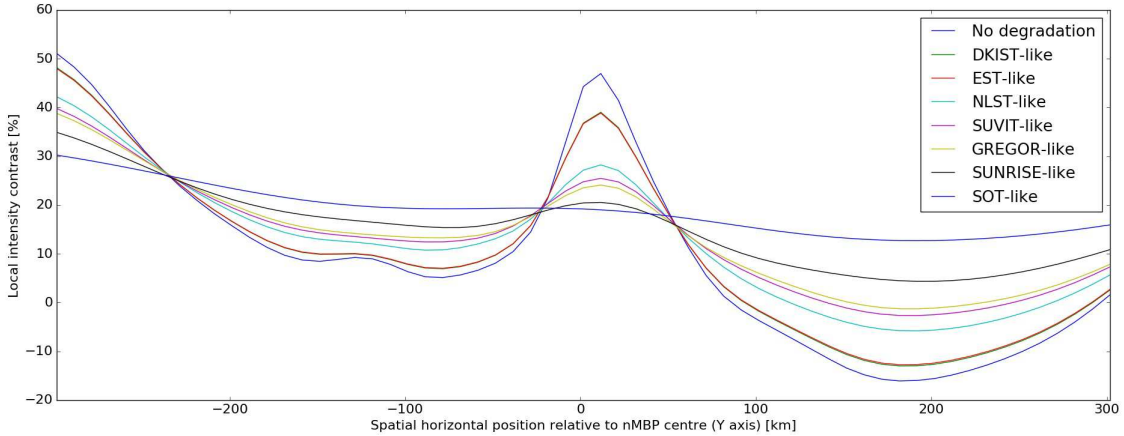

Intensity contrast across a non-magnetig bright point as observed with different telescopes.

From *Calvo et al. (2016)*.

4. *Case study II:* The discovery of non-magnetic bright points (cont.)

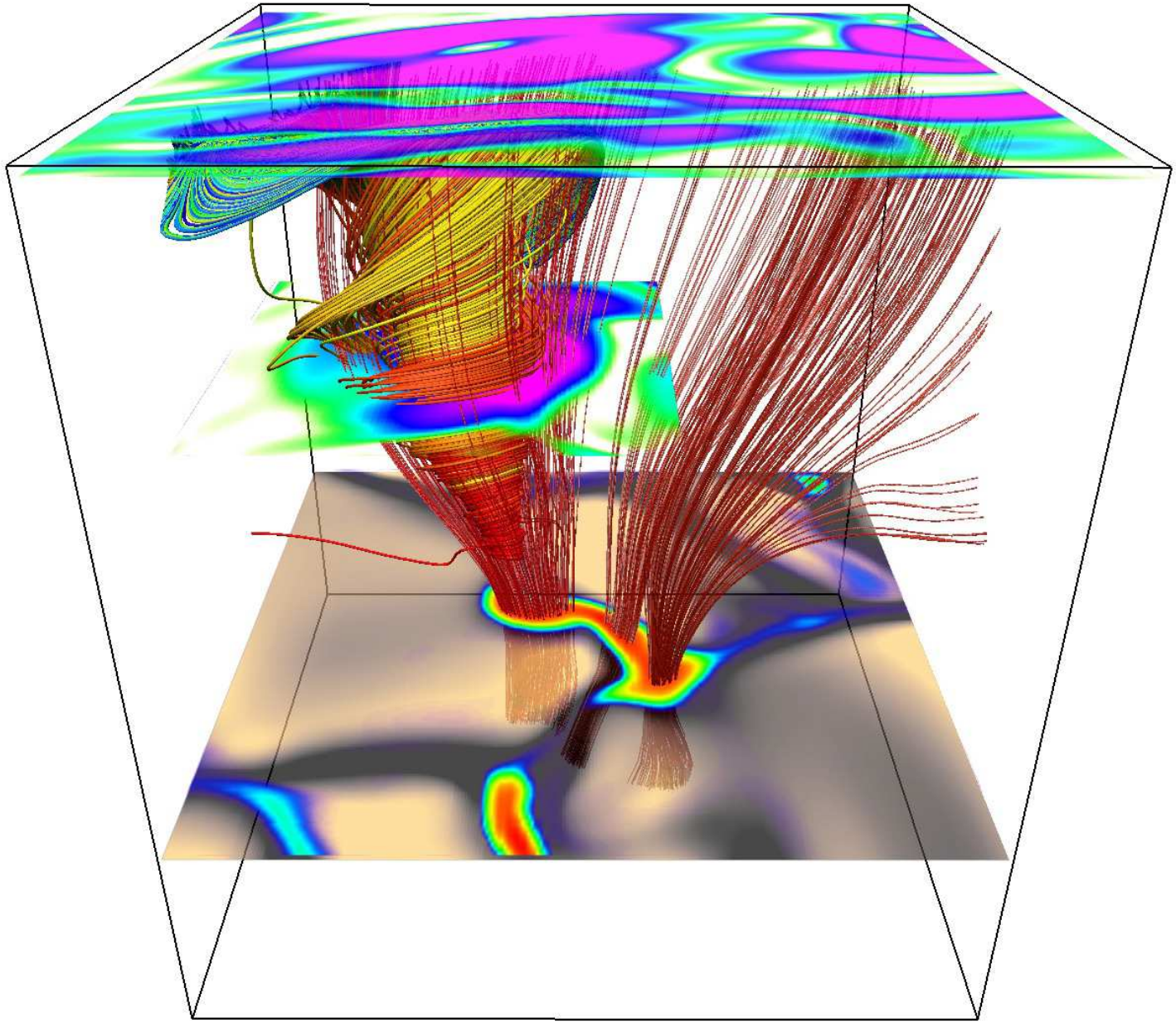

Close-up of a swirl event. The footpoints of the magnetic flux concentrations (red) are trapped in swirling downflows of the surface layers of the convection zone. In the outer atmosphere, the frozen-in plasma co-rotates with the magnetic field (spiral streamlines). From *www.solartornado.info*, *Wedemeyer et al. (2012)*

In this example, numerical simulations served to make a *prediction*. Because the simulations faithfully reproduce observed features like granules, the granular rms intensity contrast, or the shape of spectral lines, we can have some faith in the simulations. Therefore, new features, like swirling non-magnetic bright points, can, with some confidence, be predicted to really exist on the Sun. The complex structure of the non-magnetic bright points found in the simulations got *reduced to an analytical toy model*.

The next paragraph treats an example of *virtual experimentation*. Since we cannot take the Sun in the laboratory and since we cannot travel to the Sun and cary out experiments in situ, we reconstruct it in the computer for carrying out experiments.

§ 5 *Case study III:* Virtual experiments with numerical simulations

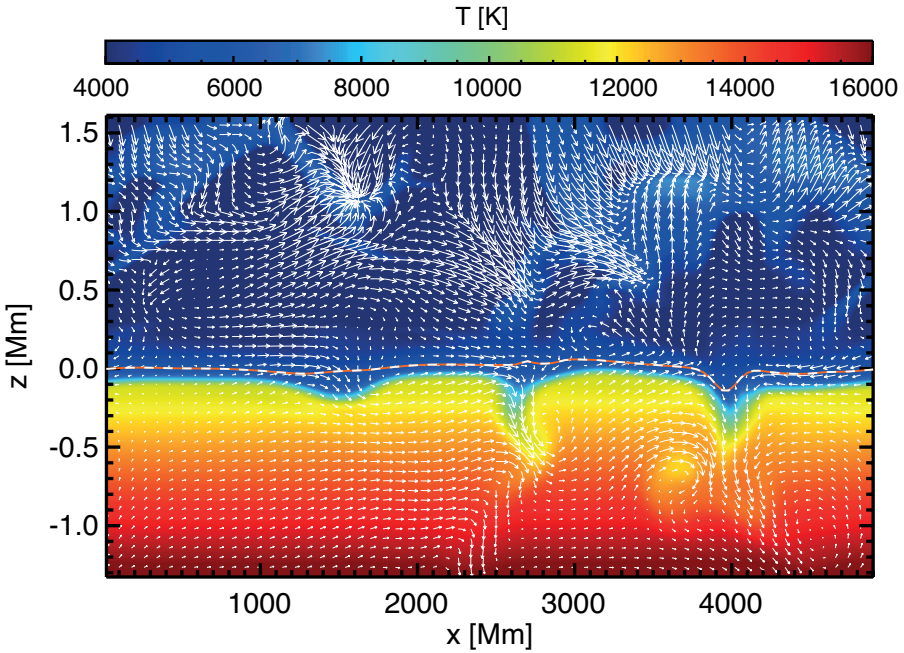

Temperature (colors), velocity (arrows), and optical depth $\tau_c = 1$ (dashed curve).

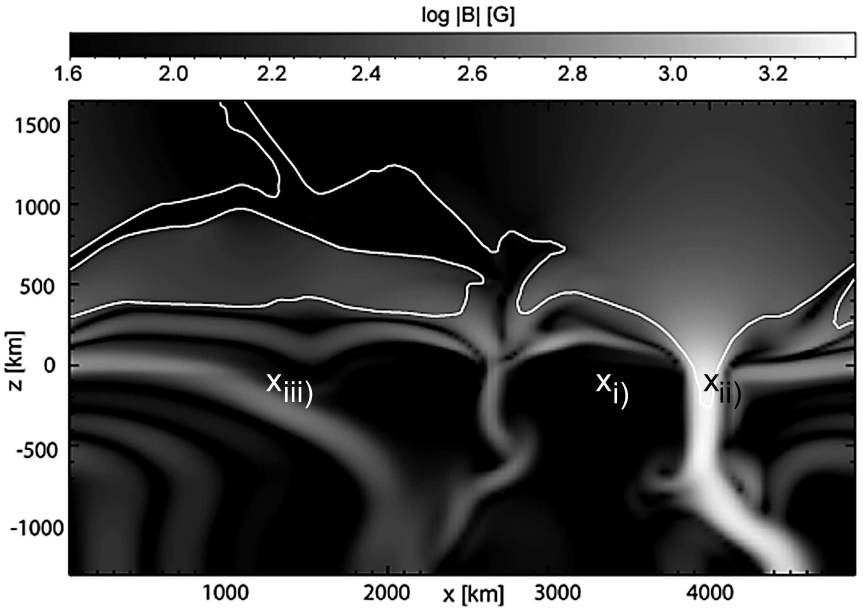

Magnetic field strength (gray scales), level where $c_s = c_A$ (white contour), locations of local wave excitation (crosses).

Movies of wave excitation at $\times_{\mathrm{i}}$, $\times_{\mathrm{ii}}$, $\times_{\mathrm{iii}}$, and along the lower boundary.

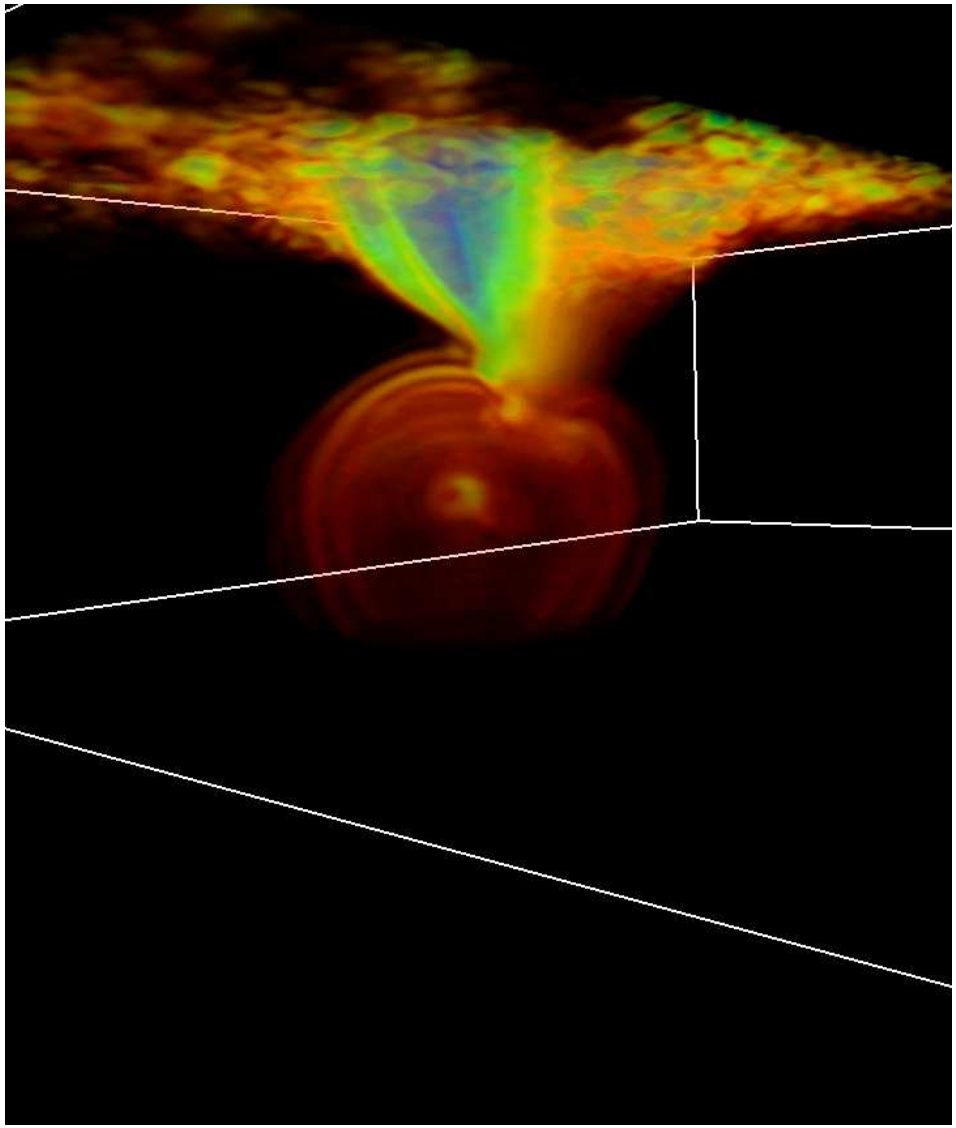

Time instant of a spherical, fast acoustic wave, initiated by a local pressure perturbation in the convection zone. When the wave encounters the low beta magnetic flux concentration in the photosphere it partially converts into a fast magnetic mode, which shows the typical “faning out” already encountered in the 2-D simulation. Colors show absolute velocity perturbation.

Courtesy *Christian Nutto, KIS*.

§ 5.1 Magnetic halos and shadows

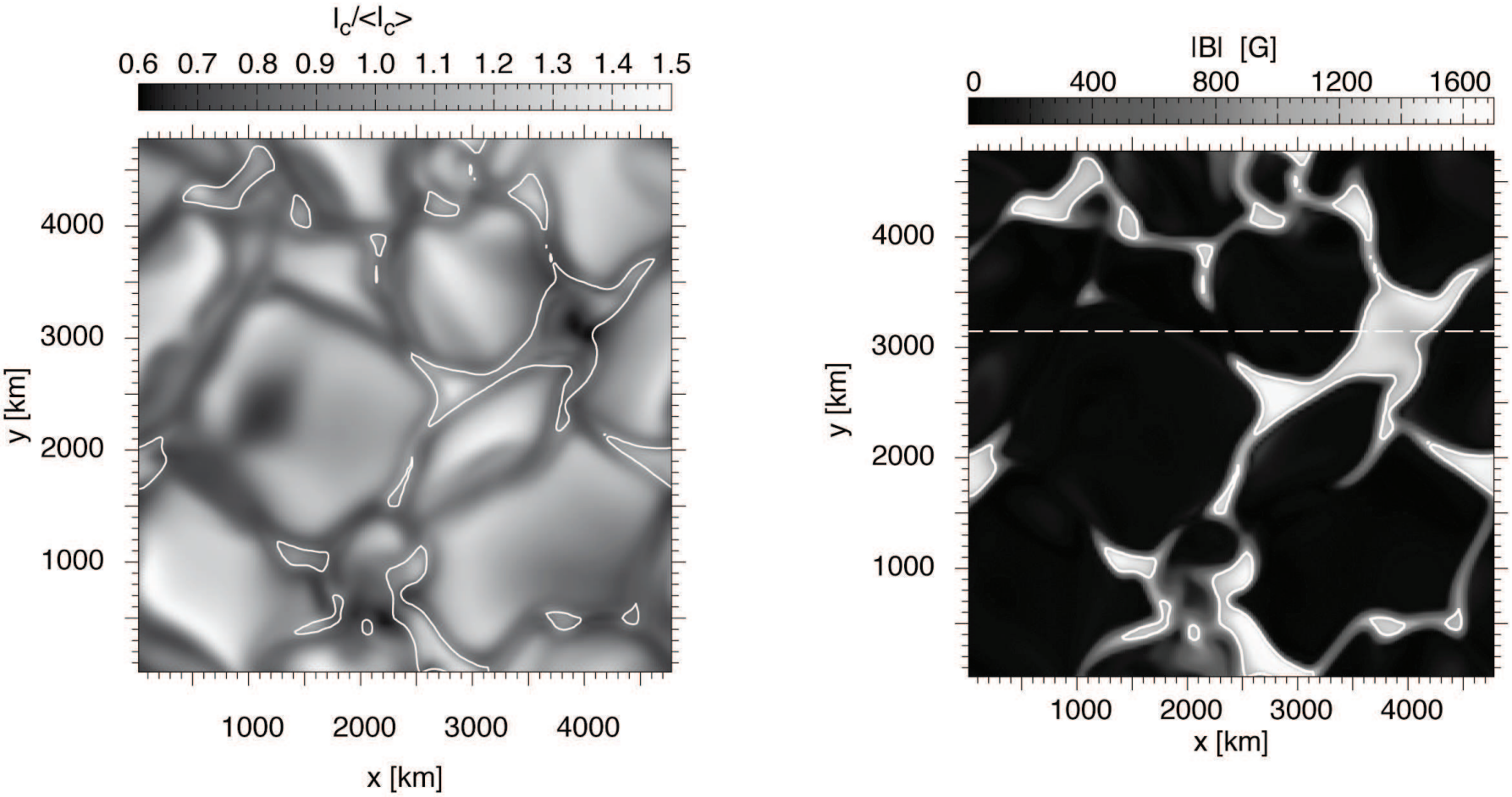

Left: FOV of $6.6'' \times 6.6''$ in white light. *Right:* Magnetic field strength at $\langle \tau_c \rangle = 1$.

Contours: Equipartition level where $c_s = c_A$. From *Nutto et al. 2012, A&A 542, L30*.

5.1. Magnetic halos and shadows (cont.)

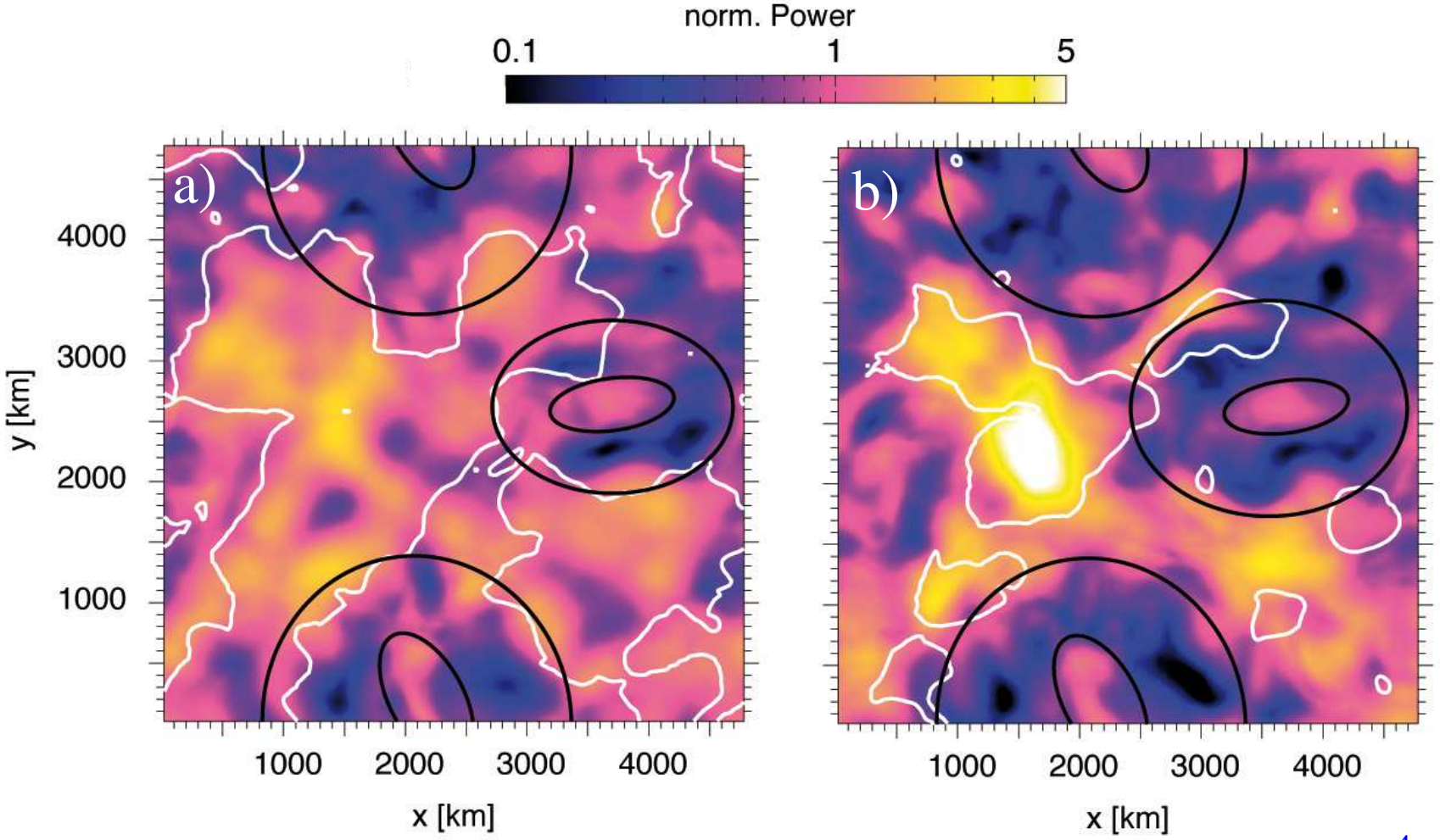

Power maps of the vertical velocity perturbations, δv_z, taken at *a)* $\tau_c = 8 \cdot 10^{-4}$ and *b)* $\tau_c = 6.7 \cdot 10^{-5}$. The *white contours* shows the equipartition level $c_s = c_A$. The *ellipses* mark regions where the *magnetic shadow* can be identified. Note suppression of power in the region between the large and the small ellipses. From *Nutto et al. 2012*.

5.1. Magnetic halos and shadows (cont.)

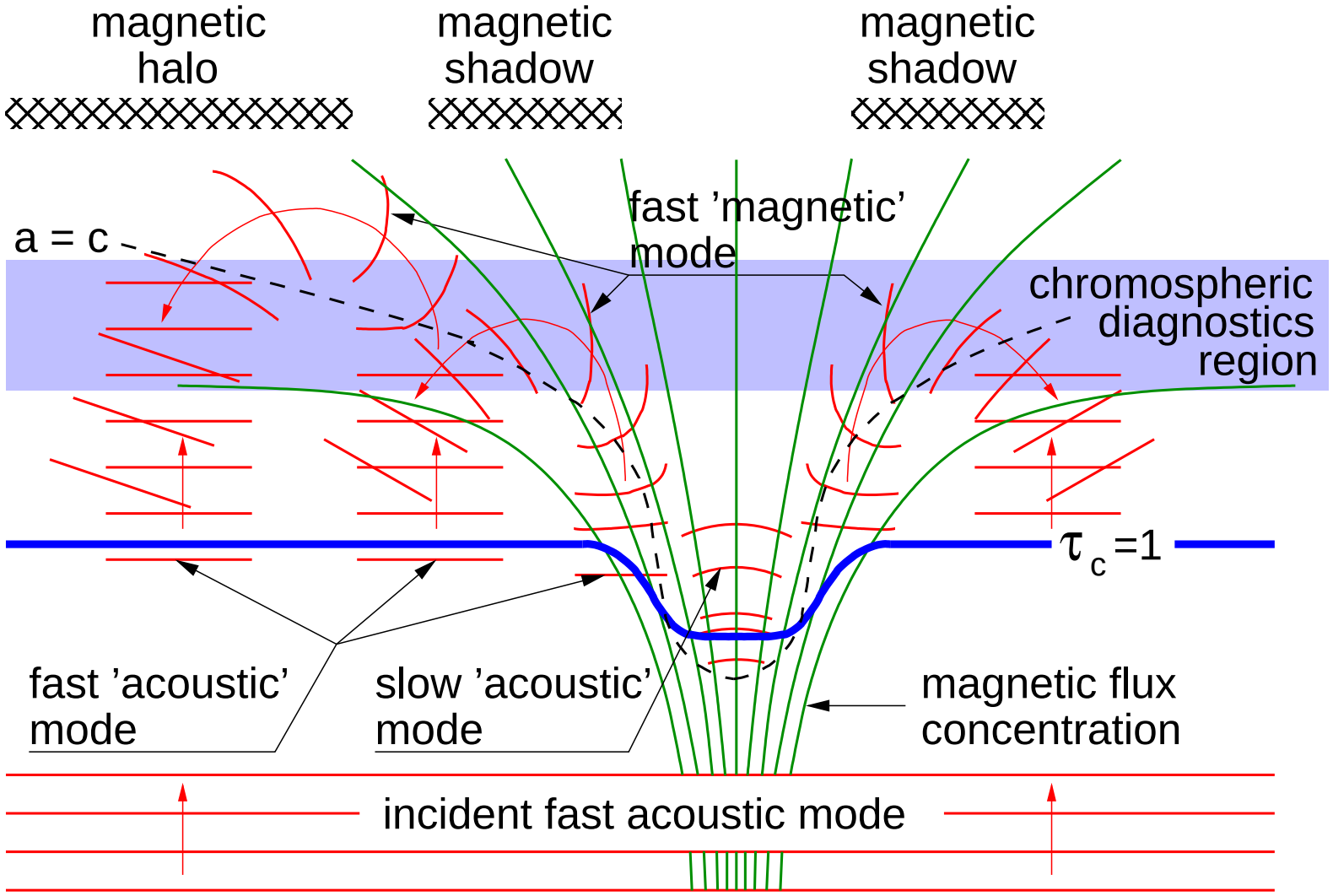

From *Komm, De Moortel, Fan, Ilonidis & Steiner, 2015 Space Sci. Rev 196, 167-199.*

Sketch of the three different magneto-acoustic modes that lead to the phenomenon of the magnetic shadow and the magnetic halo.

5.1. Magnetic halos and shadows (cont.)

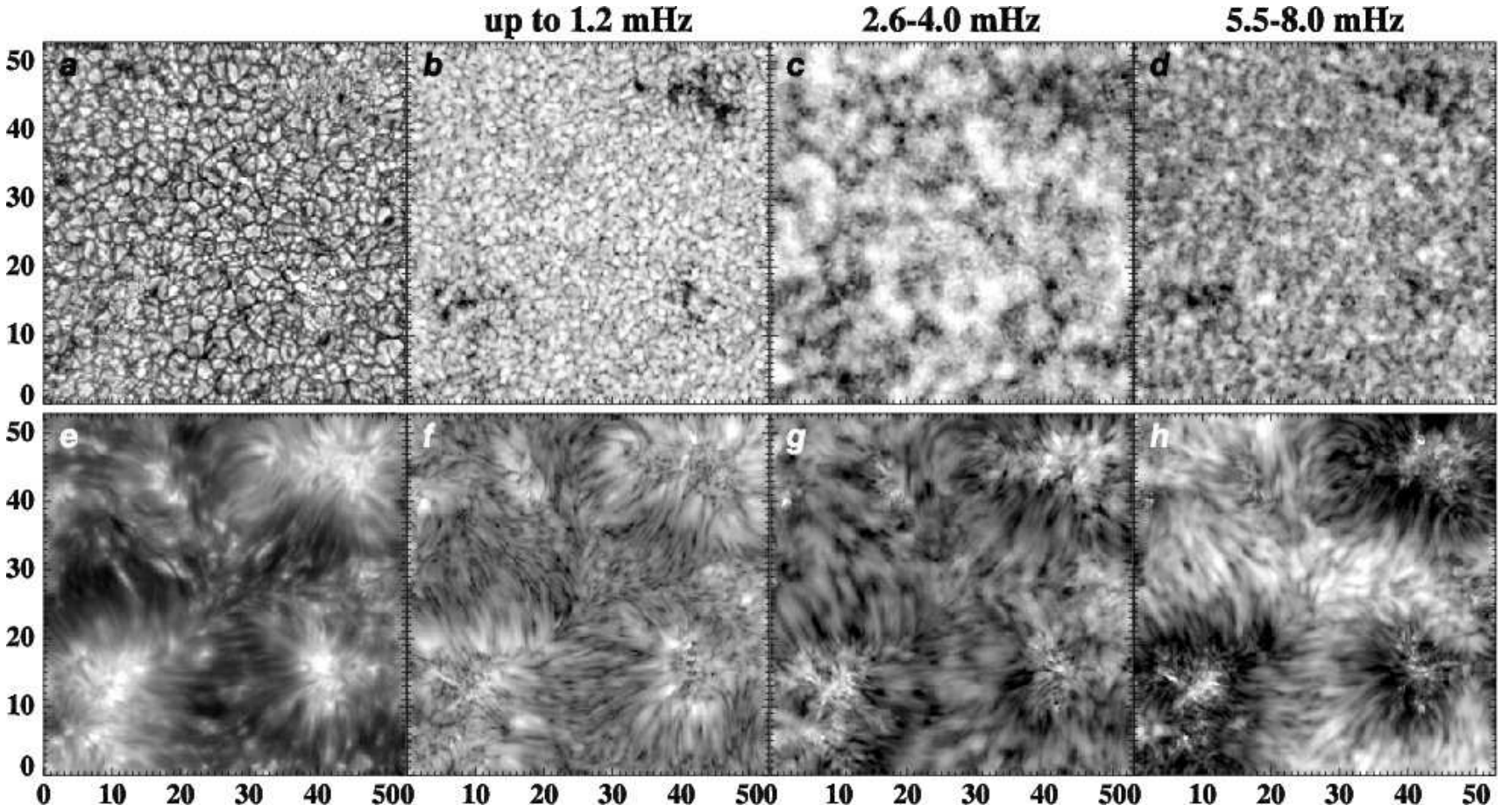

a) Broadband continuum at 710 nm. *e)* Line core intensity of CaII 854.2 nm. *b)–d)* and *f)–h)* Logarithm of the Fourier Doppler-velocity power averaged over the indicated range of frequencies of the photospheric line Fe I 709.0 nm *(b)–d))* and the chromospheric line Ca II 854.2 nm *(f)–h))*. From *Vecchio, Cauzzi, Reardon et al. (2007), A&A 461, L1.* obtained with IBIS at DST.

§ 5.2 Gravity waves

Gravity waves occur in the stable stratified (subadiabatic) part of the solar atmosphere, i.e., above the convection zone. Their restoring force is *buoyancy*. They are excited by *convective overshoot* into the photosphere.

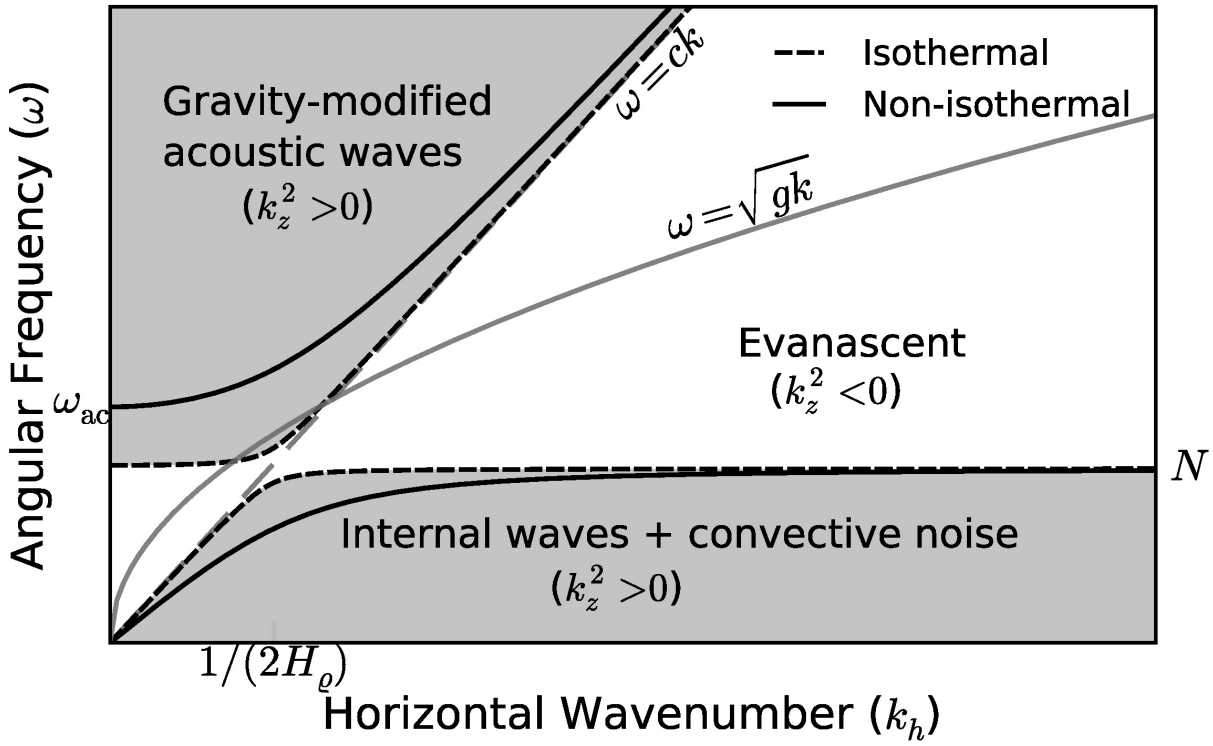

Schematic of the *diagnostic diagram* for a particular height in the atmosphere. $\omega_{\rm ac} = c_s/(2H_p)$ is the acoustic cutoff period, N the Brunt-Väisälä frequency. Internal, or gravity waves have frequencies $\omega < N$.

5.2. Gravity waves (cont.)

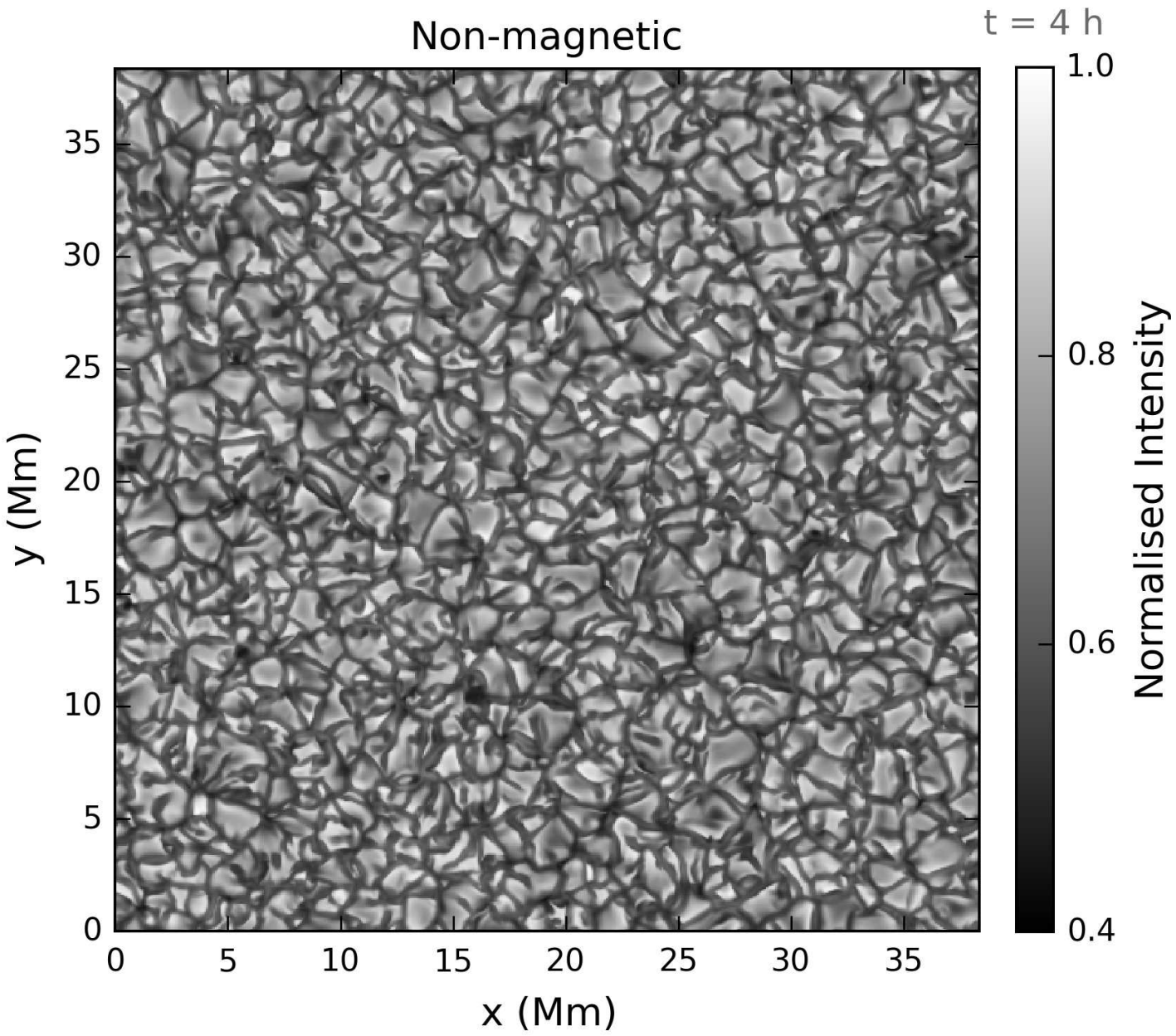

Simulation of *convective overshoot* into the stable stratified photosphere.

The simulation domain is $38.4 \times 38.4 \times 2.8$ Mm^3 and runs for 8 h physical time.

From *Vigeesh et al., 2016* in prep.

5.2. Gravity waves (cont.)

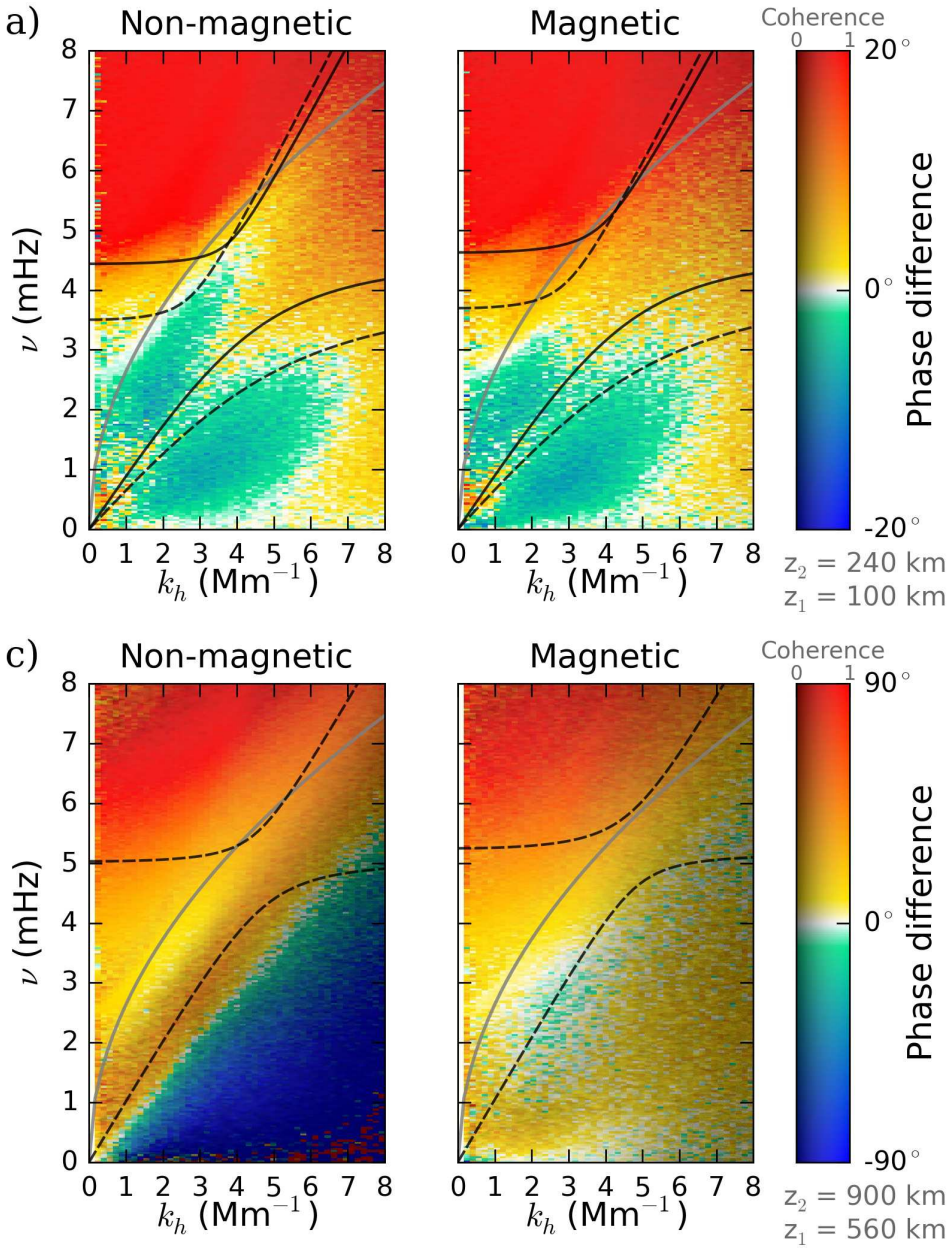

Synthetic v_z-v_z *phase difference spectra* between heights of *a)* z = 100 km and z = 240 km, *b)* z = 140 km and z = 600 km, and *c)* z = 560 km and z = 900 km, for the *non-magnetic model* (left) and the *magnetic model* (right). Note the absence of of upwardly propagating gravity waves in the upper layers of the atmosphere of the magnetic model. From *Vigeesh et al., 2016*.

5.2. Gravity waves (cont.)

Possible explanations for the absence of propagating internal waves in the upper atmosphere of the magnetic simulation are:

- *Mode conversion* of the internal wave *to Alfvén waves* (unlikely in the present case because to the predominat vertically directed magnetic field);
- Mode coupling to magneto-acoustic waves and *reflection* back into the atmosphere as described by Newington & Cally (2010, 2011).
- Non-linear interaction of internal waves with shear flows, leading to the *breaking of internal waves into turbulence*. (shear flows are provided by swirling motion in the upper atmosphere induced by the mangetic field)

§ 6 Small-scale magnetism of main sequence stellar atmospheres

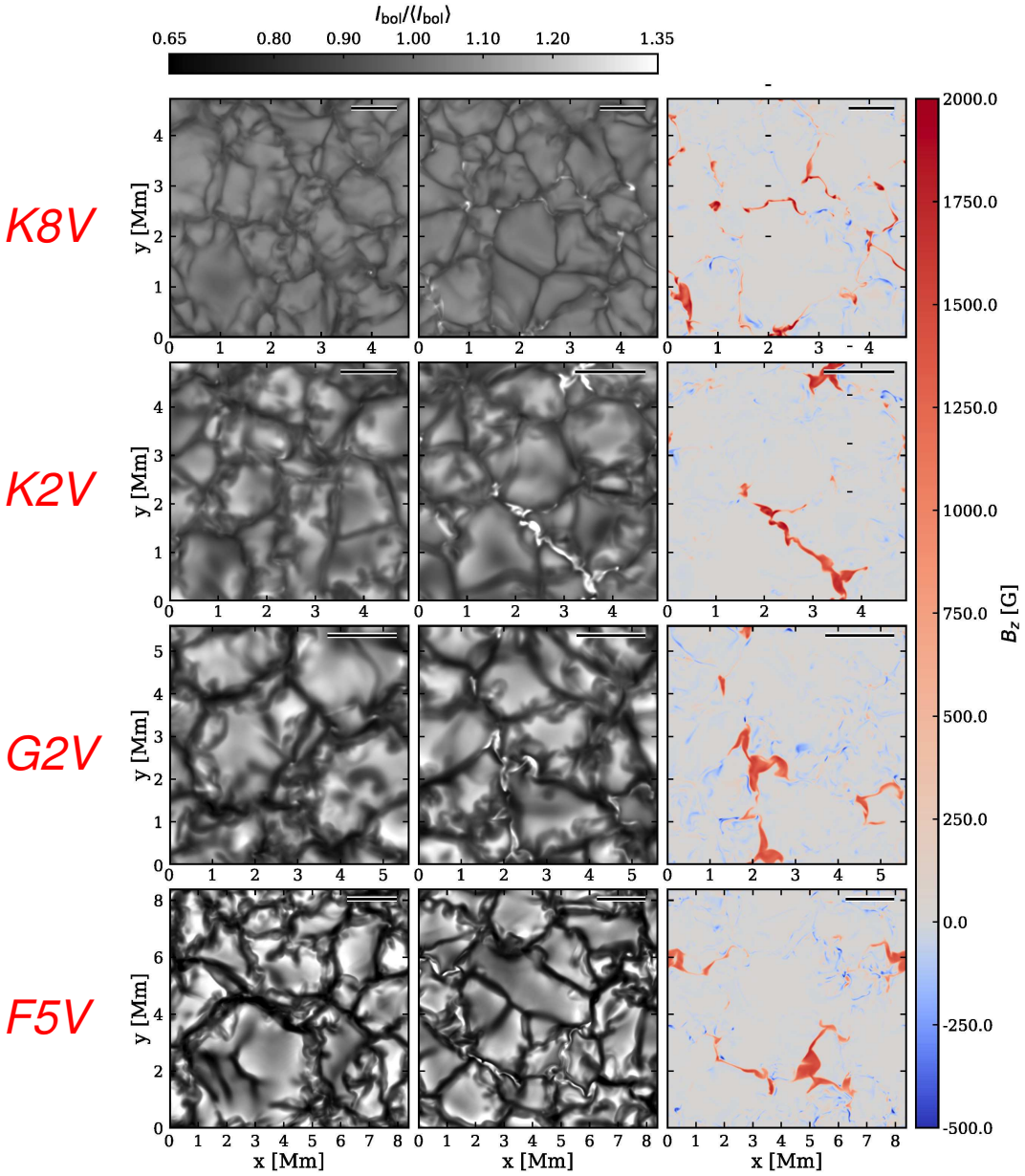

- *"Box in a star" simulations* of the surface layers of four spectral types;
- Each simulation is *run twice* : with and without magnetic fields;
- Initial vertical homogeneous field of *50 G* and *100 G* ;
- Multi-group *radiation transfer* using 5 opacity bins;
- Numerical, non-stationary, three-dimensional radiation magnetohydrodynamics using the *CO^{5}BOLD code*.

6. Small-scale magnetism of main sequence stellar atmospheres (cont.)

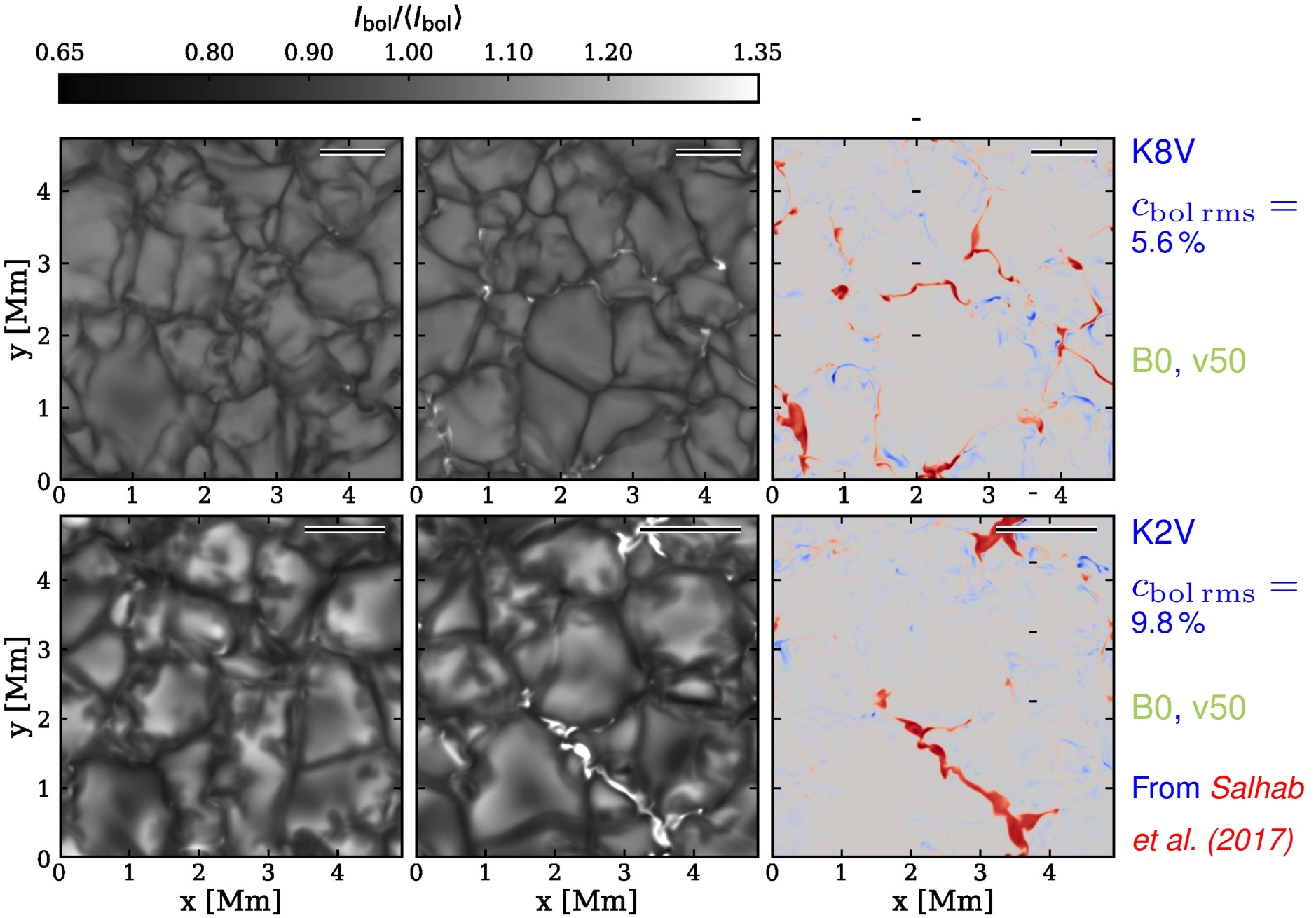

6. Small-scale magnetism of main sequence stellar atmospheres (cont.)

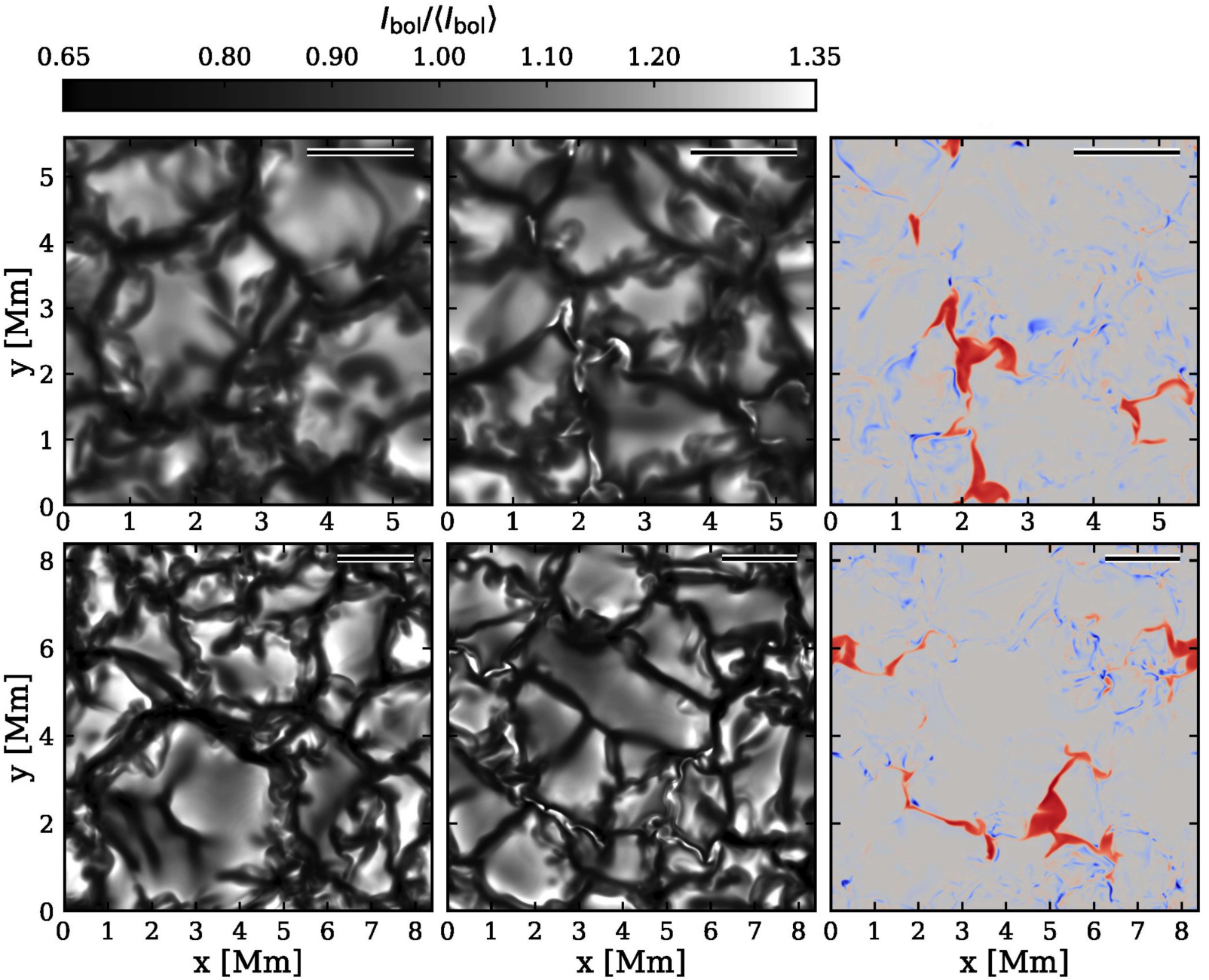

G2V

$c_{\mathrm{bol\,rms}} =$ 15.3 %

B0, v50

F5V

$c_{\mathrm{bol\,rms}} =$ 18.7 %

B0, v50

From *Salhab et al. (2017)*

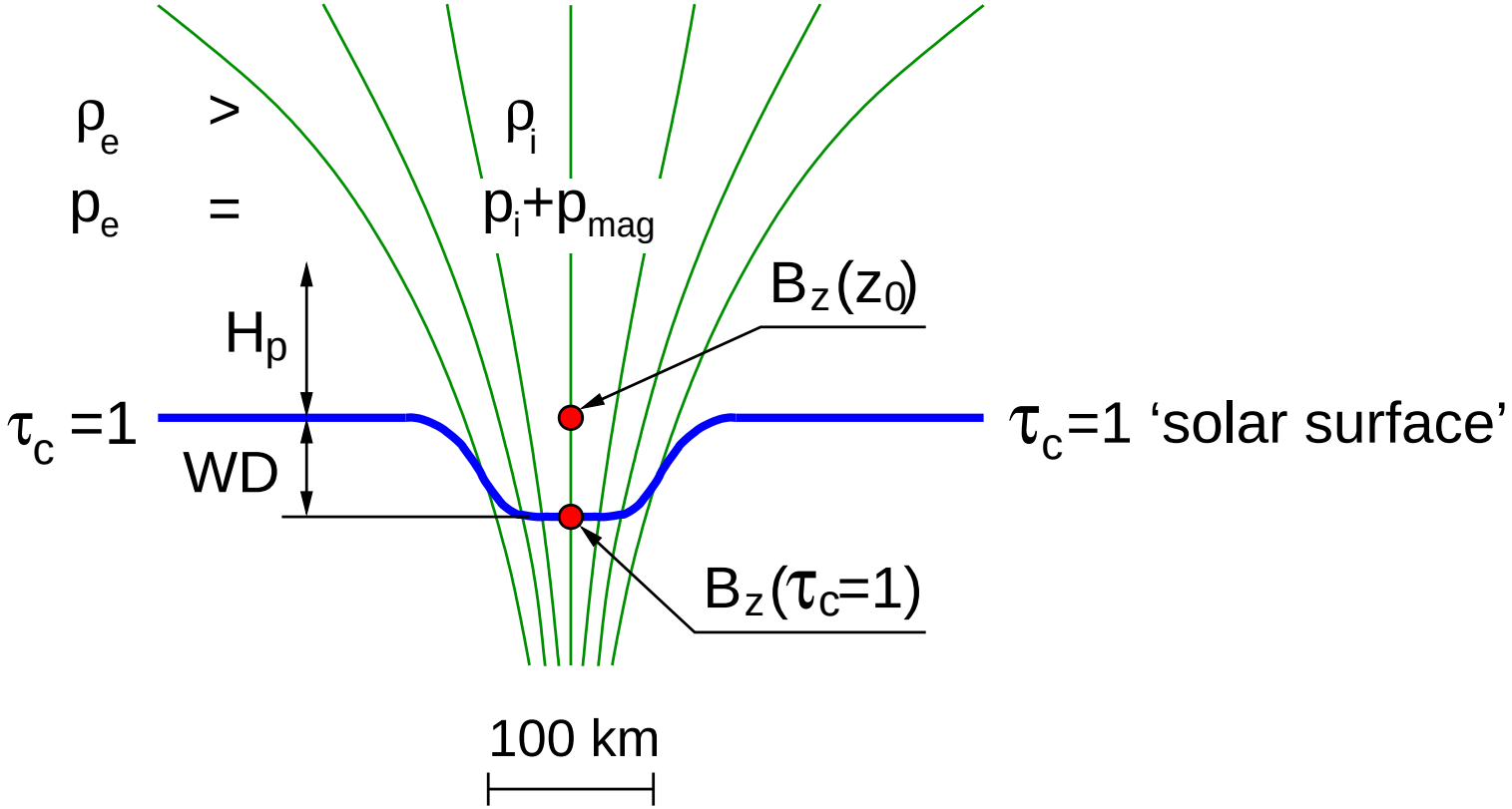

Magnetic flux concentration *(green)* with optical surface $\tau_c = 1$ *(blue)*, and "Wilson depression" WD.

	spectral type	K8V	K2V	G2V	F5V
	initial B_z [G]	50	50	50	50
1	rms$(B_{z\,\mathrm{MBF}}(z_0))$ [G]	1438 $\pm$40	1358 $\pm$42	1282 $\pm$40	1248 $\pm$32
2	*rms$(B_{z\,\mathrm{MBF}}(\tau_\mathrm{R}=1))$ [G]*	1575 $\pm$53	1598 $\pm$93	1480 $\pm$84	1565 $\pm$81
3	max$(\lvert B_{z\,\mathrm{MBF}}(z_0)\rvert)$ [G]	2204 $\pm$79	1871 $\pm$63	*1739* $\pm$73	*1675* $\pm$85
7	rms$(B_z(z_0))$ [G]	249.9 $\pm$5.5	248.0 $\pm$8.0	238.3 $\pm$7.2	237.9 $\pm$6.5
8	$p_\mathrm{gas}(z_0)$ [kPa]	*26.9* $\pm$0.1	15.2 $\pm$0.1	10.5 $\pm$0.2	*7.52* $\pm$0.2
12	$B_{\mathrm{eq\,th}}(z_0)$ [G]	2596 $\pm$5	1951 $\pm$7	*1614* $\pm$12	1362 $\pm$15
14	$B_{\mathrm{eq\,tot}}(z_0)$ [G]	2681 $\pm$5	2058 $\pm$7	1765 $\pm$11	*1550* $\pm$13
15	$\rho_\mathrm{int}/\rho_\mathrm{ext}(z_0)$ [-]	0.75 $\pm$0.02	0.54 $\pm$0.03	0.46 $\pm$0.04	0.36 $\pm$0.05
16	$\beta(z_0)$ [-]	2.7 $\pm$0.2	1.3 $\pm$0.1	0.74 $\pm$0.1	0.38 $\pm$0.1

• Constant $B_z(\tau=1)\approx 1550$ G. • *Super-equipartition magnetic fields* for F5V and partially for G2V. • Increasing evacuation with increasing T_eff.

Conclusion: • $B_{z\,\mathrm{MBF}}(\tau_{\mathrm{R}}=1)\approx 1550$ [G], fairly *independent of spectral type* • Maximal field strengths can be *superequipartition for F5* but are clearly subequipartition for K8 and K2. • The *evacuation* monotonically *increases with* increasing effective temperature, T_{eff}.

Conclusions of *Steiner, Salhab, Freytag et al. (2014), PASJ 66, S5*

Magnetic flux sheath in a

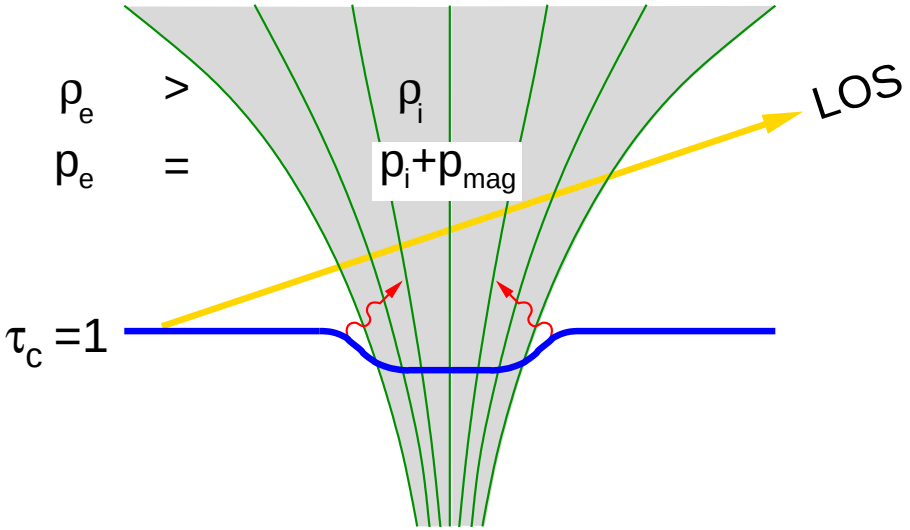

K-type atmosphere

Small depression of the $\tau_c = 1$ surface

$\Rightarrow$ *weak hot-wall effect*.

Weak evacuation

$\Rightarrow$ *faint facular granules*.

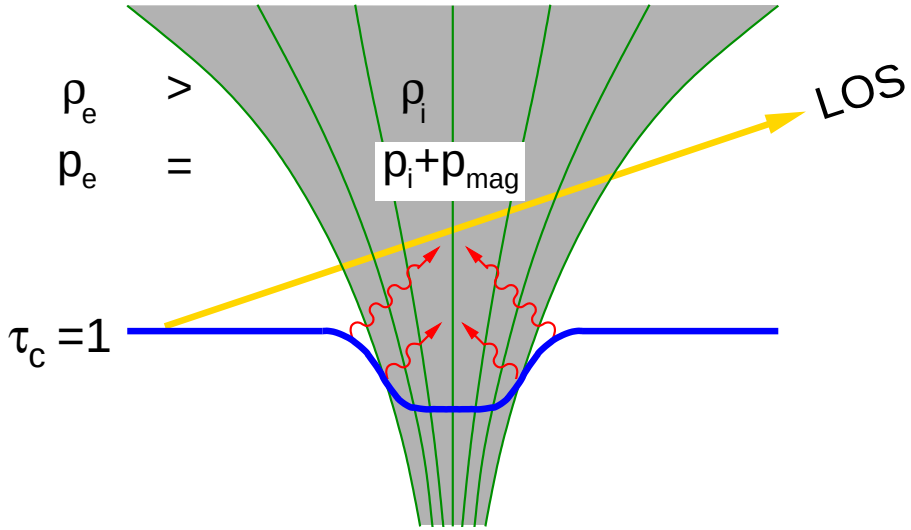

G-type atmosphere.

Large depression of the $\tau_c = 1$ surface

$\Rightarrow$ *strong hot-wall effect*.

Strong evacuation

$\Rightarrow$ *bright facular granules*.

6. Small-scale magnetism of main sequence stellar atmospheres (cont.)

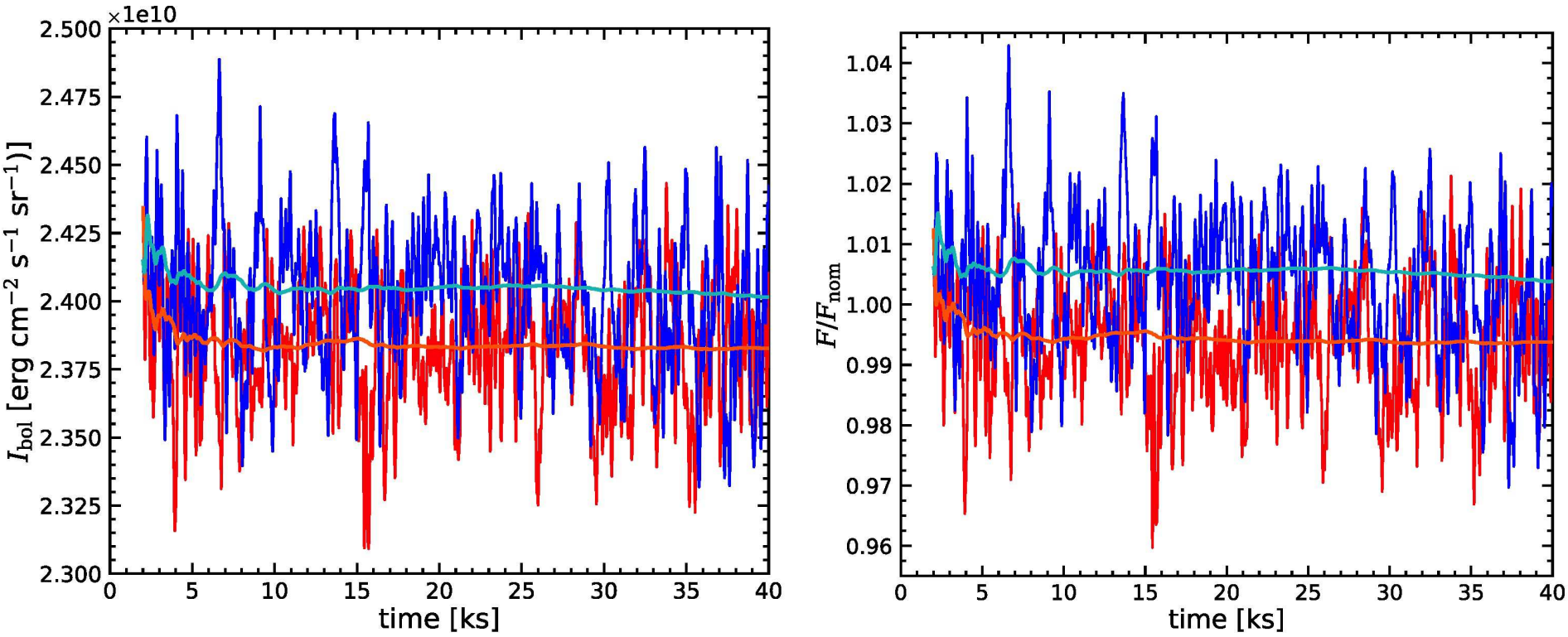

$I_{\rm bol}(t)$ (left) and $F_{\rm bol}(t)$ (right) leaving the computational domain in the vertical direction through the top boundary for the *magnetic* (*blue* curve) and the *non-magnetic* (*red* curve) *solar model (G2V)*. Cyan and orange curves are the *expanding means*.

$$I_{\rm bol}(t) = \langle I_{\rm bol}(\hat{\boldsymbol{z}},t)\rangle \;; \qquad F_{\rm bol}(t) = \left\langle \int_{4\pi} I_{\rm bol}(\boldsymbol{n},t)\,\boldsymbol{n}\cdot\hat{\boldsymbol{z}}\,{\rm d}\Omega \right\rangle .$$

	spectral type	K8V	K2V	G2V	F5V
	initial B_z [G]	50	50	50	50
25	$\delta_{I_{\rm bol}}$ [%]	0.25 $\pm$0.2	0.68 $\pm$0.9	0.88 $\pm$1.1	0.53 $\pm$0.8
26	$\delta_{F_{\rm bol}}$ [%]	*0.39* $\pm$0.2	*0.86* $\pm$0.9	*1.15* $\pm$1.1	*0.95* $\pm$0.8
27	$\delta_{F_{\rm bol}} - \delta_{I_{\rm bol}}$ [%]	0.14	0.18	0.27	0.42
30	$\mathrm{WD_w}$ [km]	60 $\pm$14	139 $\pm$34	232 $\pm$65	388 $\pm$113
31	$\mathrm{WD_w}/H_p(\tau_R = 1)$ [-]	0.7 $\pm$0.1	1.3 $\pm$0.3	1.4 $\pm$0.3	2.6 $\pm$0.7
15	$\rho_{\rm int}/\rho_{\rm ext}(z_0)$ [-]	0.75 $\pm$0.02	0.54 $\pm$0.03	0.46 $\pm$0.04	0.36 $\pm$0.05
16	$\beta(z_0)$ [-]	2.7 $\pm$0.2	1.3 $\pm$0.1	0.74 $\pm$0.1	0.38 $\pm$0.1

Radiative surplus of the magnetic over the field-free models, weighted mean *Wilson depression*, and degree of *evacuation* of the flux concentrations.

Conclusion: • For all spectral types considered here, the small-scale magnetic fields produce a *surplus in radiative intensity and flux*. It is most pronounced for G-type and early K-type stars.

• The difference $\delta_{F_{\rm bol}} - \delta_{I_{\rm bol}}$ *is always positive* and monotonically increases with increasing effective temperature, owing to the monotonically increasing Wilson depression and degree of evacuation.

References

Cally, P.S.: 2007, *What to look for in the seismology of solar active regions*, Astron. Nachr./AN 328, 286–291

Calvo, F., Steiner, O., & Freytag, B.: 2016, *Non-magnetic photospheric bright points in 3D simulations of the solar atmosphere*, A&A, submitted

De Pontieu, B., Erdélyi, R., & James, S.P. (2004), *Solar chromospheric spicules from the leakage of photospheric oscillations and flows*, Nature **430**, 536–539

Finsterle, W., Jefferies, S.M., Cacciani, A., Rapex, P., & McIntosh, S.W.: 2004, *Helioseismic mapping of the magnetic canopy in the solar chromosphere*. ApJ 613, L185–L188

Jefferies, S.M., McIntosh, S.W., Armstrong, J.D., Bogdan, T.J., Cacciani, A. & Fleck, B.: 2006, *Magnetoacoustic portals and the basal heating of the solar chromosphere*, ApJ 648, L151-L155

Judge, P.G., Tarbell, T.D., & Wilhelm, K.: 2001, *A study of chromospheric oscillations using the SOHO and TRACE spacecraft*, ApJ 554, 424

McIntosh, S.W. & Judge, P.G.: 2001, *On the nature of magnetic shadows in the solar chromosphere*, ApJ 561, 420

Komm, R., De Moortel, I., Fan, Y., Ilonidis, S. and Steiner, O.: 2015, *Sub-photosphere to Solar Atmosphere Connection*, in Helioseismology and Dynamics of the Solar Interior, J. Len Culhane et al. (eds.), Space Science Reviews 196, 167-199

Michalitsanos, A.G.: 1973, *The Five Minute Period Oscillation in Magnetically Active Regions*, Sol. Phys. 30, 47–61

Newington, M.E. and Cally, P.S. 2010, MNRAS, 402, 386

Nutto, C., Steiner, O., & Roth, M.: 2012, *Revealing the nature of magnetic shadows with numerical 3D-MHD simulations*, A&A, 542, L30

Nutto, C., Steiner, O., Schaffenberger, W., & Roth, M.: 2012, *Modification of wave propagation and wave travel-time by the presence of magnetic fields in the solar network atmosphere*, A&A 538, A79

Riethmller, T. L., Solanki, S. K., Martínez Pillet et al.: 2010, *Bright Points in the Quiet Sun as Observed in the Visible and Near-UV by the Balloon-borne Observatory SUNRISE*, ApJL 723, L169-L174

Salhab, R.G., Steiner, O., Berdyugina, S.V.: 2017, *Simulation of the small-scale magnetism in main sequence stellar atmospheres*, A&A, in prep.

Suematsu, Y.: 1990, *Influence of Photospheric 5-Minute Oscillations on the Formation of Chromospheric Fine Structures*, in *Progress of Seismology of the Sun and Stars*, Osaki, Y., & Shibahashi, H., eds., Lecture Notes in Physics, Berlin Springer Verlag, **367**, 211–214

Steiner, O. & Rezaei, R.: 2012, *Recent Advances in the Exploration of the Small-Scale Structure of the Quiet Solar Atmosphere: Vortex Flows, the Horizontal Magnetic Field, and the Stokes-V Line-Ratio Method*, in L. Golub, I. De Moortel, and T. Shimizu (eds.), Hinode 5: Exploring the Active Sun, ASP Conf. Ser. 456, p. 3-32.

Stenflo, J.O.: 2010, *Distribution functions for magnetic fields on the quiet Sun*, A&A 517, A37

Vecchio, A., Cauzzi, G., Reardon, K. P., Janssen, K., & Rimmele, T.: 2007, *Solar atmospheric oscillations and the chromospheric magnetic topology*, A&A 461, L1

Vigeesh, G., Jackiewicz, J., and Steiner, O.: 2016, *Internal gravity waves in the magnetized solar atmosphere: I. Magnetic field effects*, ApJ, in prep.

Wiehr, E., Bovelet, B., and Hirzberger, J.: 2004, *Brightness and size of small-scale solar magnetic flux concentrations*, A&A, 422, L63-L66

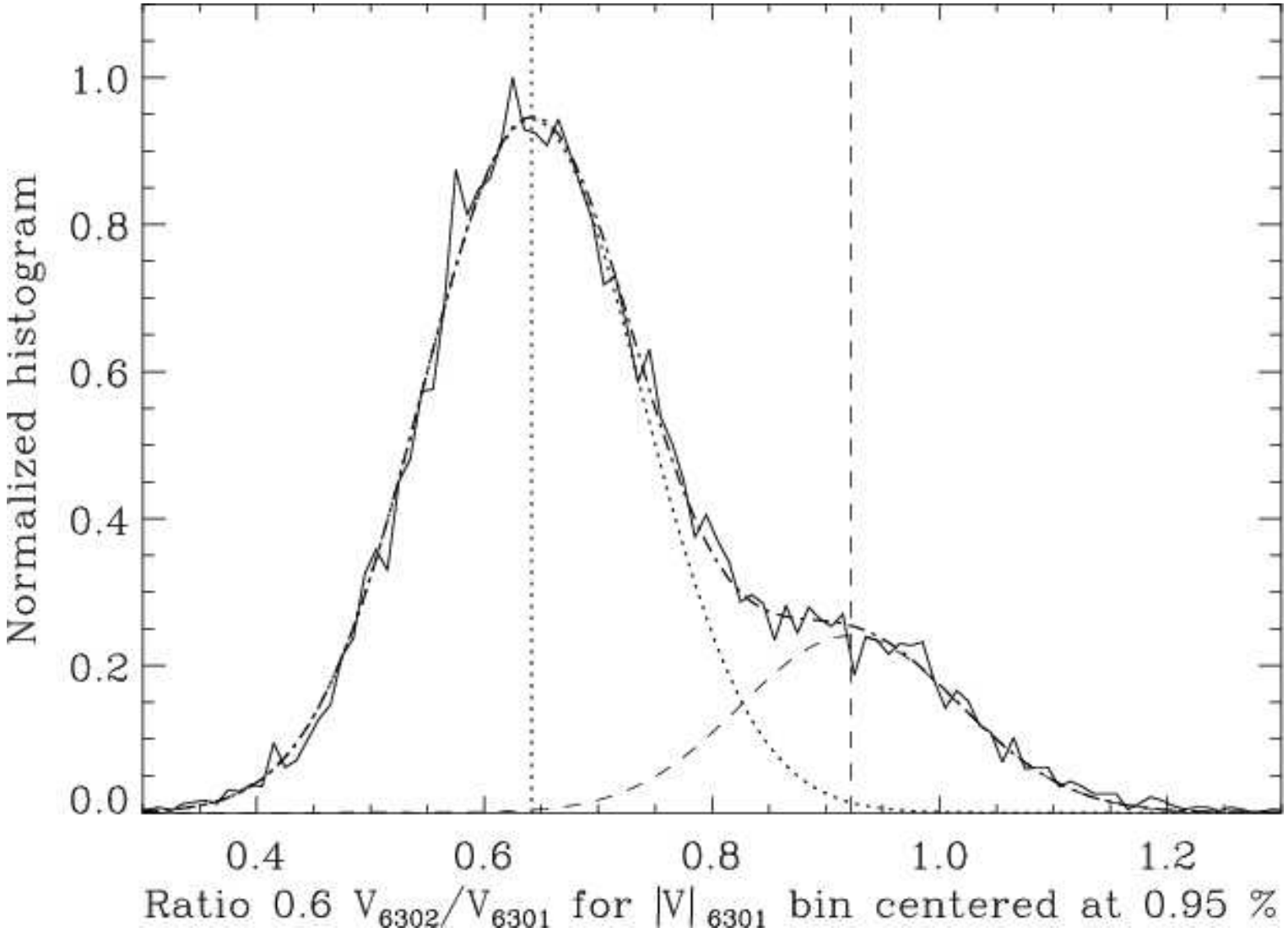
Normalized histogram
1.0
0.8
0.6
0.4
0.2
0.0
0.4
0.6
0.8
1.0
1.2
Ratio 0.6 V_{6302}/V_{6301} for $|V|_{6301}$ bin centered at 0.95 %

→ backto § 2.